

# WRF/Chem-MADRID: Incorporation of an aerosol module into WRF/Chem and its initial application to the TexAQS2000 episode

Yang Zhang,<sup>1</sup> Ying Pan,<sup>1</sup> Kai Wang,<sup>1</sup> Jerome D. Fast,<sup>2</sup> and Georg A. Grell<sup>3,4</sup>

Received 25 October 2009; revised 16 February 2010; accepted 14 April 2010; published 17 September 2010.

[1] The Model of Aerosol Dynamics, Reaction, Ionization and Dissolution (MADRID) with three improved gas/particle mass transfer approaches (i.e., bulk equilibrium (EQUI), hybrid (HYBR), and kinetic (KINE)) has been incorporated into the Weather Research and Forecast/Chemistry Model (WRF/Chem) (referred to as WRF/Chem-MADRID) and evaluated with a 5-day episode from the 2000 Texas Air Quality Study (TexAQS2000). WRF/Chem-MADRID demonstrates an overall good skill in simulating surface/aloft meteorological parameters and chemical concentrations of O<sub>3</sub> and PM<sub>2.5</sub>, tropospheric O<sub>3</sub> residuals, and aerosol optical depths. The discrepancies can be attributed to inaccuracies in meteorological predictions (e.g., overprediction in mid-day boundary layer height), sensitivity to meteorological schemes used (e.g., boundary layer and land-surface schemes), inaccurate total emissions or their hourly variations (e.g., HCHO, olefins, other inorganic aerosols) or uncounted wildfire emissions, uncertainties in initial and boundary conditions for some species (e.g., other inorganic aerosols, CO, and O<sub>3</sub>) at surface and aloft, and some missing/inactivated model treatments for this application (e.g., chlorine chemistry and secondary organic aerosol formation). Major differences in the results among the three gas/particle mass transfer approaches occur over coastal areas, where EQUI predicts higher PM<sub>2.5</sub> than HYBR and KINE due to improperly redistributing condensed nitrate from chloride depletion process to fine PM mode. The net direct, semi-direct, and indirect effects of PM<sub>2.5</sub> decrease domainwide shortwave radiation by 11.2–14.4 W m<sup>-2</sup> (or 4.1–5.6%) and near-surface temperature by 0.06–0.14°C (or 0.2–0.4%), lead to 125 to 796 cm<sup>-3</sup> cloud condensation nuclei at a supersaturation of 0.1%, produce cloud droplet numbers as high as 2064 cm<sup>-3</sup>, and reduce domainwide mean precipitation by 0.22–0.59 mm day<sup>-1</sup>.

**Citation:** Zhang, Y., Y. Pan, K. Wang, J. D. Fast, and G. A. Grell (2010), WRF/Chem-MADRID: Incorporation of an aerosol module into WRF/Chem and its initial application to the TexAQS2000 episode, *J. Geophys. Res.*, 115, D18202, doi:10.1029/2009JD013443.

## 1. Introduction

[2] Atmospheric aerosols affect climate through directly absorbing and scattering of solar radiations (i.e., direct effects) and indirectly changing planetary boundary layer (PBL) meteorology variables that depend on radiation (i.e., semi-direct effects) and altering the formation of clouds and precipitation by serving as cloud condensation nuclei (CCN) (i.e., indirect effects). Their distributions and formation

mechanisms are governed by many atmospheric processes including gas-phase chemistry, aerosol thermodynamic and dynamic processes, cloud processes, and dry and wet deposition. Among these processes, gas/particle mass transfer process plays an important role in determining aerosol mass concentrations. Three gas/particle mass transfer approaches (i.e., bulk equilibrium, kinetic (or dynamic), and hybrid) are commonly used in three dimensional (3-D) Air Quality Models (AQMs). The bulk equilibrium and hybrid approaches are computationally more efficient but less accurate under certain conditions (e.g., when the concentrations of reactive coarse particles are high), whereas the kinetic approach is more accurate but computationally is slow [Zhang *et al.*, 1999; Hu *et al.*, 2008]. Several studies compared the differences between two or three gas/particle mass transfer approaches using a box model [e.g., Capaldo *et al.*, 2000; Hu *et al.*, 2008], a 1-D model [e.g., Koo *et al.*, 2003], and 3-D models [e.g., Gaydos *et al.*, 2003; Tombette and Sportisse,

<sup>1</sup>Department of Marine, Earth and Atmospheric Sciences, North Carolina State University, Raleigh, North Carolina, USA.

<sup>2</sup>Pacific Northwest National Laboratory, Richland, Washington, USA.

<sup>3</sup>Earth Systems Research Laboratory, NOAA, Boulder, Colorado, USA.

<sup>4</sup>Also at CIRES, University of Colorado at Boulder, Boulder, Colorado, USA.

2007]. The studies examining sensitivity of model predictions to the three approaches using 3-D models, however, are limited to a few episodes and geographical domains (e.g., the southern California and France), and the use of offline-coupled models. Computationally efficient yet accurate kinetic approaches have been developed in several studies [e.g., *Jacobson, 2005; Hu et al., 2008; Zaveri et al., 2008*].

[3] Unlike most 3-D AQMs, the Weather Research and Forecast/Chemistry Model (WRF/Chem) is an online-coupled meteorology-air quality model that can simulate meteorology-chemistry-aerosol-cloud-radiation feedbacks via direct, semi-direct, and indirect effects. WRF/Chem version 3.0 includes several gas-phase mechanisms (e.g., Regional Acid Deposition Model, version 2 (RADM2) [*Stockwell et al., 1990*] and Carbon-Bond Mechanism version Z (CBM-Z) [*Zaveri and Peters, 1999*]) and several aerosol modules (e.g., the Modal Aerosol Dynamics Model for Europe (MADE) with the secondary organic aerosol model (SORGAM) of *Schell et al. [2001]* (referred to as MADE/SORGAM) and the Model for Simulating Aerosol Interactions and Chemistry (MOSAIC) [*Zaveri et al., 2008*]). WRF/Chem with RADM2 and MADE/SORGAM was first applied for the summer 2002 NEAQS field study and demonstrated a better skill in forecasting O<sub>3</sub> than MM5/Chem [*Grell et al., 2005*]. It has also been used for the ensemble forecast of O<sub>3</sub> [*McKeen et al., 2005*] and PM<sub>2.5</sub> [*McKeen et al., 2007*] and for the evaluation of the impacts of emission reductions on O<sub>3</sub> in the eastern U.S. [*Frost et al., 2006*]. WRF/Chem with CBM-Z and MOSAIC has been applied to a 5-day episode from the 2000 Texas Air Quality Study (TexAQS) (referred to as TexAQS2000) and demonstrated a good skill in simulating O<sub>3</sub> and aerosols and aerosol shortwave radiative forcing [*Fast et al., 2006*]. In this work, the improved version of the model of aerosol dynamics, reaction, ionization and dissolution (MADRID) of *Zhang et al. [2004]* as described by *Hu et al. [2008]* and *Hu [2008]* has been incorporated into WRF/Chem v3.0 (released in April 2008) and evaluated using the same TexAQS2000 episode of *Fast et al. [2006]* over the Houston-Galveston, Texas area. Our objectives are to improve WRF/Chem's capabilities in simulating aerosols, evaluate WRF/Chem-MADRID using the TexAQS2000 observations, examine the sensitivity of aerosol predictions to different gas/particle mass transfer approaches, and demonstrate the model's capability in estimating aerosol direct and indirect effects.

## 2. Description of the Episode, Model, and Evaluation Protocol

### 2.1. Episode Description

[4] Houston, Texas is the 4th most populous city in the U.S. with four-million people. Traffic and other local anthropogenic sources such as the Houston Ship Channel and petrochemical industries result in high emission rates of nitrogen oxides (NO<sub>x</sub>) and volatile organic compounds (VOCs). 40% of the world's production capacity of low molecular weight alkenes is estimated to be produced in the Houston-Galveston area [*Daum et al., 2004*]. Depending on the wind direction, the emissions of isoprene and monoterpenes from the forested regions in the northeast of Houston and sea-salt emissions from the Gulf of Mexico also contribute to the total emissions in this area. The O<sub>3</sub> mixing ratios

in Houston often exceed the 1-h National Ambient Air Quality Standard (NAAQS) of 120 ppb [*Daum et al., 2003*] and the 8-h NAAQS of 80 ppb. Under favorable weather conditions, the O<sub>3</sub> formation in Houston is rather rapid and some high O<sub>3</sub> events are observed even when background O<sub>3</sub> level is modest [*Daum et al., 2004*], making the O<sub>3</sub> problem in Houston rather unique. Exceedance of an annual PM<sub>2.5</sub> NAAQS of 15 μg m<sup>-3</sup> has also been a concern [*Russell et al., 2004*]. Direct emissions in this area contribute to ~40–50% of particulate matter with aerodynamic diameters equal to or less than 2.5 μm (PM<sub>2.5</sub>) while secondary sources account for 50–60% of PM<sub>2.5</sub> with inorganic species dominating the secondary PM [*Russell and Allen, 2004; Pavlovic et al., 2006; Allen and Fraser, 2006*].

[5] In August and September of 2000, the TexAQS2000 was conducted to improve the understanding of the formation and transport of the pollutants such as O<sub>3</sub> and PM<sub>2.5</sub> along the Gulf Coast of the southeastern TX. Intensive measurements of gaseous, PM, and hazardous air pollutants were made at ~20 ground stations, located throughout the eastern half of TX. The characteristics of air pollutants have been examined through both field [e.g., *Kleinman et al., 2002, 2005; Ryerson et al., 2003; Wert et al., 2003; Daum et al., 2003; Karl et al., 2003; Russell et al., 2004; Banta et al., 2005; Murphy and Allen, 2005; Allen and Fraser, 2006; Webster et al., 2007*] and modeling studies [e.g., *Chang et al., 2002; Tanaka et al., 2003; Jiang and Fast, 2004; Darby, 2005; Nam et al., 2006; Chang and Allen, 2006; Fast et al., 2006; Misenis and Zhang, 2010*].

[6] In this study, a 5-day (1200 GMT August 28–0600 GMT September 2) episode from the TexAQS2000 is used as an initial testbed for the evaluation of WRF/Chem-MADRID. There are several reasons for selecting this 5-day period. First, more than 20 1-h O<sub>3</sub> exceedances were observed during this period in the Houston-Galveston-Brazoria area, 6 of them exceeded 150 ppb. Second, sea breezes were observed during August 29–31, 2000, which are typically associated with high O<sub>3</sub> events in the Houston area [*Banta et al., 2005; Darby, 2005*]. Such events would provide the most stringent case to test the model's capability in replicating the frequent occurrences of sea breezes and their impact on elevated O<sub>3</sub>. Third, some gas/particle mass transfer approaches may fail to predict the distribution of semi-volatile species for areas where anthropogenic emissions are mixed with sea-salt emission. The high percentage of secondary PM and the mixing of sea-salt and anthropogenic emissions during this episode make the TexAQS2000 episode a good testbed to compare the three gas/particle mass transfer approaches in WRF/Chem-MADRID.

### 2.2. Model Description

[7] MADRID is an aerosol module that treats all major aerosol chemical and microphysical processes including inorganic aerosol thermodynamic equilibrium, secondary organic aerosol (SOA) formation, nucleation, condensation, gas/particle mass transfer, and coagulation. As described by *Zhang et al. [2004]*, ISORROPIA v1.6 of *Nenes et al. [1998]* is used to simulate inorganic aerosol thermodynamic equilibrium. SOA formation is treated using two formulations: an empirical representation (referred to as MADRID 1) that is based on a reversible absorption theory and smog chamber data, and a mechanistic representation (referred to

as MADRID 2) that simulates both hydrophilic and hydrophobic particles. The number of condensable species is 38 in MADRID 1 and 42 in MADRID 2. The homogeneous binary nucleation of sulfuric acid and water vapor is simulated using the approach of *McMurry and Friedlander* [1979] that accounts for the competition between nucleation and condensation. Gas/particle mass transfer is simulated with three algorithms: a bulk equilibrium approach that assumes full equilibrium between gas and particulate phases, a hybrid approach that treats mass transfer explicitly for coarse particles and assumes full equilibrium for fine particles, and a kinetic approach that solves the full aerosol dynamic equation. Condensation is implicitly treated by allocating the transferred mass to different size sections based on the condensational growth law in the bulk equilibrium approach but explicitly simulated based on the growth law of *Capaldo et al.* [2000] in the hybrid and the kinetic approaches. The growth of particles over sections with fixed size boundaries due to various growth processes (e.g., condensation, and aqueous-phase chemistry) in all three approaches is simulated using the moving-center scheme of *Jacobson* [2005]. *Hu et al.* [2008] updated ISORROPIA v1.6 to v1.7 in MADRID and adapted the noniterative, unconditionally stable analytical predictor of condensation (APC) of *Jacobson* [2005] to replace the condensational growth law of *Capaldo et al.* [2000].

[8] An updated version of MADRID that was described by *Zhang et al.* [2004, 2010a] and *Hu et al.* [2008] has been incorporated into WRF/Chem v3.0 and coupled with several gas-phase mechanisms such as CBM-Z, the 2005 Carbon Bond Mechanism (CB05), and the 1999 Statewide Air Pollution Research Center (SAPRC) mechanism and the Carnegie Mellon University (CMU) aqueous-phase chemistry. Compared with previous versions, several major modifications have been made in MADRID in this study. First, the number of surrogates of SOA compounds has been reduced from 38 (4 anthropogenic and 34 biogenic) to 25 (7 anthropogenic and 18 biogenic) based on *Pun et al.* [2005] to simulate SOA more efficiently. SOA formation from the oxidation of isoprene, monoterpenes, and sesquiterpene is accounted for. Second, the coagulation algorithm of *Jacobson et al.* [1994] has been incorporated into MADRID 1 to provide a more realistic representation of PM<sub>2.5</sub> number concentrations and size distribution as described by *Zhang et al.* [2010a]. This coagulation code conserves total particle volume and volume concentration and is positive-definite, non-iterative, and stable. Third, different from *Hu et al.* [2008] in which nucleation process was deactivated and water vapor was assumed to instantly equilibrate with particles, the updated MADRID in this study simulates binary nucleation of sulfuric acid and water vapor and explicitly treats condensation/evaporation for water vapor. Compared with MADE/SORGAM that uses a modal size representation in WRF/Chem, MADRID uses a sectional size representation and differs in nearly all aspects in terms of aerosol thermodynamic and dynamic treatments. Compared with MOSAIC that also uses a sectional size representation and a dynamic approach for gas/particle mass transfer but does not yet simulate SOA, MADRID uses different modules for simulating inorganic aerosol thermodynamics, nucleation, condensation, and subsequent growth, simulates SOA, and offers three approaches to simulate gas/particle mass transfer. MADRID uses the same aqueous-phase chemistry and aerosol direct

and indirect effect treatments as those for MOSIAC as described by *Fast et al.* [2006] and *Chapman et al.* [2008].

### 2.3. Model Setup and Evaluation Protocol

[9] WRF/Chem-MADRID simulations are conducted for a region of  $1056 \times 1056 \text{ km}^2$  with a 12-km horizontal grid spacing and 56 layers from surface to 100 mb. Twenty-eight layers are used from surface to 2.85 km to resolve boundary layer meteorological processes. Model input data (i.e., emissions and meteorological and chemical initial and boundary conditions (ICONS and BCONs)) are based on *Fast et al.* [2006]. ICONs and BCONs for PM<sub>2.5</sub> concentrations within 2 km above the surface are set to be  $8 \mu\text{g m}^{-3}$  based on available measurements, which is proportionally reduced above 2 km. They are set horizontally homogeneous, which is justified because PM<sub>2.5</sub> concentrations and composition are found to be generally spatially homogeneous throughout the southeastern TX on a seasonal average [*Russell et al.*, 2004; *Allen and Fraser*, 2006]. As indicated by *Fast et al.* [2006], the size of this domain does not account for long-range transport (LRT) of pollutants; however, observed pollution was largely caused by local anthropogenic and biogenic emission sources because the meteorological conditions during this period were not favorable for LRT (although LRT may affect the abundance of pollutants in upper troposphere). The gaseous emissions including those from the offshore stationary sources and maritime traffic were provided by the Texas Commission on Environmental Quality (TCEQ). The PM emissions were obtained from the EPA's 1999 National Emissions Inventory (NEI) version 3. Eight size sections over  $0.0215 \mu\text{m}$ – $10 \mu\text{m}$  are used to represent the aerosol size distribution. Major physics options used include the Goddard shortwave radiation scheme, the rapid and accurate radiative transfer model (RRTM) for longwave radiation, the Fast-J photolysis rate scheme, the Yonsei University (YSU) planetary boundary layer (PBL) scheme, and the National Center for Environmental Prediction, Oregon State University, Air Force, and Hydrologic Research Lab's (NOAH) land-surface scheme, the modified Purdue Lin microphysics module, and the Grell-Devenyi cumulus parameterization. The CBM-Z gas-phase mechanism, the MADRID aerosol module, and the CMU aqueous-phase chemistry are used. The coupling of CBM-Z with MADRID does not allow the simulation of SOA in this study because SOA condensable precursors cannot be directly added into CBM-Z that is hard-wired in WRF/Chem. Simulations are conducted with three gas/particle mass transfer approaches, i.e., the bulk equilibrium, hybrid/APC, and kinetic/APC approaches (referred to as WRF/Chem-MADRID (EQUI), (HYBR), and (KINE), respectively). All simulations include aerosol direct and indirect effects. While EQUI is considered as a baseline simulation, the results from HYBR and KINE will provide the sensitivity of the model predictions to different gas/particle mass transfer processes. An additional simulation that does not treat aerosol emissions and its microphysical and chemical processes is conducted to examine the aerosol feedbacks into radiation, PBL meteorology, and cloud and precipitation formation. The differences in model predictions between this additional simulation and the baseline simulation are caused by cloud-aerosol interactions and differences in the auto-conversion scheme used in both simulations.

**Table 1.** Observational Data Sets Used for Model Evaluation

Networks	Variables or Species	Data Frequency	Number of Sites
AIRS <sup>a</sup>	O <sub>3</sub>	1-h	102
CASTNET <sup>a</sup>	O <sub>3</sub>	1-h	2
TCEQ <sup>a</sup>	Wind speed and direction at 10-m (WS10 and WD10), temperature and relative humidity at 2-m (T2 and RH2), PBL height (PBLH), O <sub>3</sub> , PM <sub>2.5</sub>	1-h	32 sites for T2; 31 sites for WS10 and WD10; 7 sites for RH2; 5 for PBLH; 60 for O <sub>3</sub> ; 15 for PM <sub>2.5</sub>
NCDC	WS10, T2, RH2, and Precip	Daily average for WS10, T2, and RH2, Daily total for Precip	93 sites
NOAA/NCAR Electra aircraft	Vertical profiles of temperature, relative humidity, CO, NO, NO <sub>2</sub> , O <sub>3</sub>	1-s	N/A
NARR <sup>a</sup>	Precipitation, WS10, WD10, T2, and RH2	3-h	Domainwide
AERONET <sup>a</sup>	Aerosol optical depth (AOD)	1-h	1
MODIS <sup>a,b</sup>	AOD	One data at 10:30 A.M. per day	Domainwide
TOMS <sup>a</sup>	Tropospheric Ozone Residue (TOR)	1-day	Domainwide

<sup>a</sup>AERONET: Aerosol Robotic Network; AIRS: the Aerometric Information Retrieval System; CASTNET: the Clean Air Status and Trends Network; MODIS: the MODerate resolution Imaging Spectroradiometer; NARR: the North American Regional Reanalysis; TCEQ: the Texas Commission on Environmental Quality; NCDC: National Climatic Data Center; TOMS/SBUV: Total Ozone Mapping Spectrometer/Solar Backscattered UltraViolet.

<sup>b</sup>MODIS data used in this study is taken from the Terra satellite. Its overpass time is at 10:30 A.M., LST.

[10] The observational data used for model evaluation are summarized in Table 1. The data sets include meteorological and chemical measurements from TeXAQS2000 provided by the TCEQ, meteorological measurements from National Climatic Data Center (NCDC), surface chemical data from the U.S. EPA's routine networks such as the Aerometric Information Retrieval System (AIRS) and the Clean Air Status and Trends Network (CASTNET), aircraft measurements from the NOAA/NCAR Electra during TeXAQS2000, remote-sensed measurements including the Total Ozone Mapping Spectrometer (TOMS)/Solar Backscattered UltraViolet (SBUV), the MODerate resolution Imaging Spectroradiometer (MODIS), and the lidar-based Aerosol Robotic Network (AERONET). The variables evaluated include meteorological variables such as temperature at 2-m (T2), relative humidity at 2-m (RH2), wind speed and wind direction at 10 m (WS10 and WD10), daily precipitation (Precip), and PBL height (PBLH), the surface concentrations of O<sub>3</sub> and PM<sub>2.5</sub>, the vertical profiles of temperature, RH, and mixing ratios of CO, NO, NO<sub>2</sub>, and O<sub>3</sub>, as well as Tropospheric Ozone Residual (TOR) and Aerosol optical depth (AOD). Most published model applications to TeXAQS2000 largely focused on surface and near-surface variables, fewer studies assessed the model's capability in reproducing vertical profiles of meteorological and chemical variables. The simulated profiles of meteorological variables and chemical concentrations are extracted along the flight tracks to compare with their observed vertical profiles from the NOAA/NCAR Electra aircraft during TeXAQS 2000. The flight observations below 4 km were made within half an hour in coastal areas. Simulated profiles are extracted from the hourly model output that is the closest to the time of observations in different grid cells along the flight track. No study evaluated the column variables such as TOR and AOD from satellite data and examined aerosol indirect studies during this episode. AODs at a wavelength of 0.55  $\mu\text{m}$  are retrieved from the level 3 MODIS/Terra products with a grid resolution of  $10 \times 10 \text{ km}^2$  and used to compare with model predictions. In this work, model predictions at 10:00 A.M. and 11:00 A.M.

local standard time (LST) are extracted and averaged to obtain predictions at 10:30 A.M. for comparison with the MODIS-derived AODs from Terra that has an overpass time of 10:30 A.M. LST. In addition, the assimilated meteorological predictions of wind fields, temperatures, RHs, and precipitation from the North American Regional Reanalysis (NARR) as well as wind field observations from literature are also used for model evaluation.

[11] Figure 1 shows the modeling domain and locations of all observational sites for meteorology, surface O<sub>3</sub>, and PM<sub>2.5</sub> by the TCEQ. The evaluation is conducted in terms of spatial distribution, temporal variation, vertical profile, and performance statistics. The main statistical metrics used for model evaluation include: correlation coefficient (corr), mean bias (MB), root mean square error (RMSE), normalized mean bias (NMB), and normalized mean error (NME), mean normalized bias (MNB), and mean normalized gross error (MNGE). Formulas for these metrics are given by *Seigneur et al.* [2000] and *Zhang et al.* [2006].

### 3. Evaluation of Baseline Simulation Results From WRF/Chem-MADRID (EQUI)

#### 3.1. Meteorological Predictions

[12] Several studies have indicated that the meteorological processes (e.g., sea breeze, low-level jets) play a vital role in O<sub>3</sub> events in Houston [*Banta et al.*, 2005; *Darby*, 2005]. Meteorological predictions are therefore evaluated to assess the model's capability to accurately reproduce observations, which will affect its performance in capturing the O<sub>3</sub> events in terms of time of occurrence, location, and peak values. Different simulations (i.e., EQUI, HYBR, and KINE) will give different meteorology due to different aerosol direct and indirect feedbacks. Such feedbacks, however, are overall similar, therefore only the meteorological predictions from EQUI are evaluated.

[13] *Daum et al.* [2003] showed an observed dominance of the westerly in the Houston-Galveston area in the morning. A sea breeze developed around noon time. The front of the

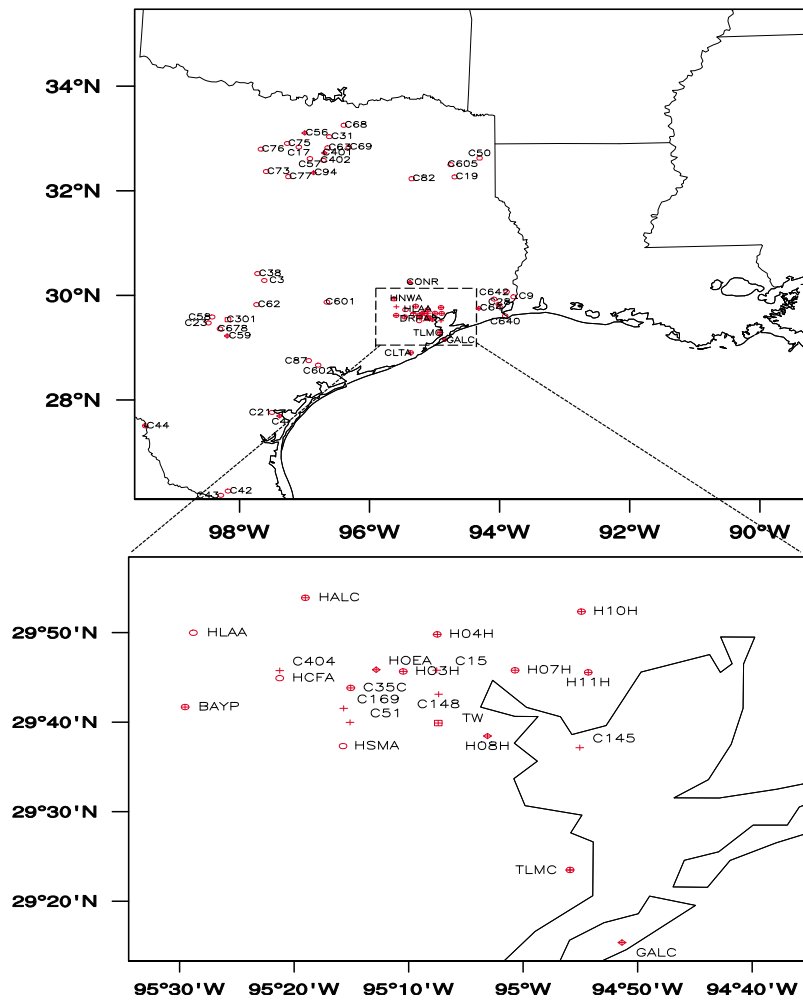


**Figure 1.** The 12-km modeling domain and locations of meteorology,  $O_3$ , and  $PM_{2.5}$  observational sites (32, 60, and 15, respectively) from the TCEQ in (top) the modeling domain and (bottom) in the Houston-Galveston area. The symbols are as follows: circles,  $O_3$  only sites; squares, PM only sites; diamonds,  $O_3$  and PM co-located sites; and pluses, meteorological sites.

sea breeze reached the Houston area at 12 CST and a confluence line formed, when the wind field was nearly stagnant in this area. The sea breeze continued to develop in the afternoon, with its front reaching further inland until 18 CST. Figure 2 shows simulated surface wind fields at 8, 10, 12, 16, and 18 central standard time (CST) on August 29. The observed sea breeze development throughout August 29 is well reproduced by EQUI, although the predicted strength of the sea breeze is not as strong as that from observations. Lack of penetration of the sea breeze is also reported from other model simulations [e.g., Angevine *et al.*, 2006; Fast *et al.*, 2006]. The bias of the predicted sea breezes is shown to be partially caused by improper grid resolution [Colby, 2004]. A horizontal grid resolution of 12 km used here may be too coarse to capture the local-scale atmospheric thermodynamics and dynamics around the Houston area. Such a coarse resolution also cannot well represent land use and land cover, which is critical to accurately predict the PBL meteorology [Grossman-Clarke *et al.*, 2005]. Discrepancies between the actual land use and that used in the model are suspected to contribute to the model biases in the predictions of land-sea

temperature, winds, and PBLH reported by Bao *et al.* [2005]. WRF/Chem uses the 24-category U.S. Geological Survey (USGS) land use and land cover data set. Because the use of a coarse grid resolution, the division of land mask and land use does not match exactly with the coastal line, especially around Galveston Bay (e.g., some land areas are modeled as water area and vice versa) (not shown). This mismatching will lower the model skill in capturing the sea breezes, especially over Houston where the coastline is rather inhomogeneous.

[14] Figure 3 shows the temporal variations of wind vectors at 10-m height at 10 sites selected from 31 sites: Continuous Ambient Monitoring Station 56 in Denton Airport South, Dallas-Fort Worth (CMAS56), Conroe (CONR), Houston Aldine (HALC), Houston Bayland Park (BAYP), Houston East (HOEA), Clinton (C35C), Houston Deer Park (DRPA), LaPorte (H08H), Texas City (TLMC), and Galveston Airport (GALC). Most sites are located in Houston or its vicinity (within 15 miles of downtown Houston) except that CMAS56 and CONR are located 279.1 and 40.6 miles, respectively, northwest of Houston, and TLMC and GALC are located

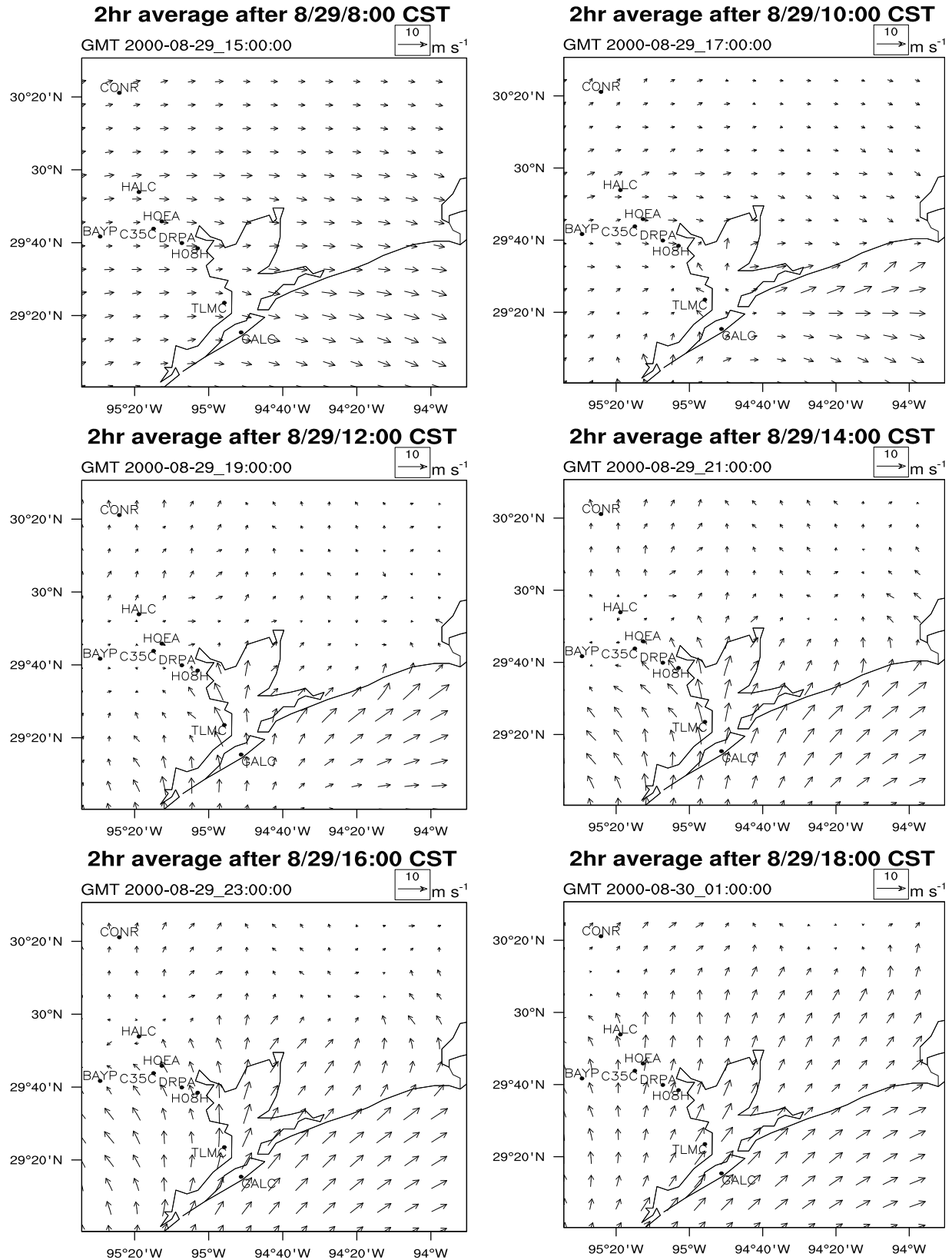


**Figure 2.** Predicted wind fields by WRF/Chem-MADRID (EQUI) on Aug. 29, 2000. The locations of meteorological sites in the Houston-Galveston area shown in Figures 3–5 are plotted in the background.

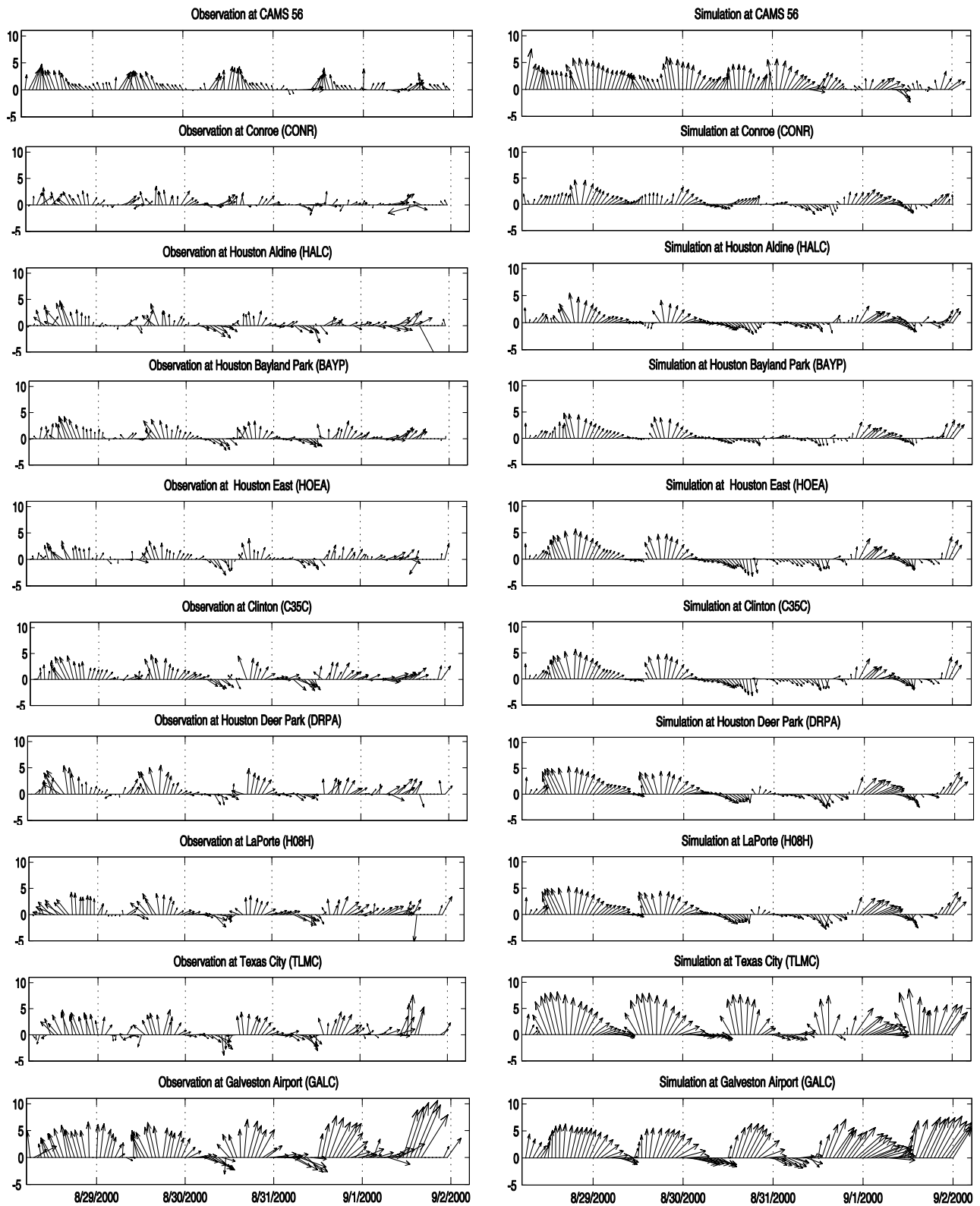


Figure 3. Observed and simulated temporal variations of wind vectors at 10 sites. The simulated results are from WRF/Chem-MADRID (EQU).

**Table 2.** Performance Statistics of Hourly Predictions by WRF/Chem-MADRID (EQUJ)<sup>a</sup>

	T2 (°C)		RH2 <sup>b</sup> (%)		WS10 (m s <sup>-1</sup> )		WD10 (deg)		PBLH (m)		Precip <sup>c</sup> (mm day <sup>-1</sup> )		O <sub>3</sub> (ppb)		PM <sub>2.5</sub> (µg m <sup>-3</sup> )		TOR (Du)		AOD	
	TCEQ	NCDC	TCEQ	NCDC	TCEQ	NCDC	TCEQ	NCDC	TCEQ	NCDC	TCEQ	NCDC	AQS + CASTNET+TCEQ	TCEQ	TCEQ	TOMSS	MODIS			
MeanObs	31.2	30.8	62.5	35.8	2.9	5.6	210.0	1089.3	0.37	0.37	39.3	10.3	42.7	0.27						
MeanMod	31.8	31.9	44.2	41.6	3.3	3.2	230.5	1915.4	0.42	0.42	39.9	13.0	53.5	0.21						
Number	3500	369	793	346	3389	368	3389	203	366	6234	1682	7744	6418	7744						
corr	0.9	0.5	0.7	0.8	0.3	0.6	0.5	0.6	-0.03	0.6	0.2	0.2	0.3	0.75						
MB	0.5	1.1	-18.3	5.7	0.3	-2.4	20.5	826.1	0.06	0.6	0.6	2.7	10.8	-0.06						
RMSE	2.0	2.5	25.2	15.2	1.8	3.3	70.9	1086.9	3.1	16.4	16.4	8.7	11.6	0.1						
NMB (%)	1.7	3.5	-29.2	16.0	11.6	-43.9	9.8	75.8	15.2	1.4	1.4	26.4	25.3	-23.2						
NME (%)	5.0	5.9	31.1	35.7	48.6	48.3	21.5	79.8	210.5	30.5	30.5	59.9	25.3	25.4						
MNB (%)	2.0	4.0	-26.8	120.1	71.6	-30.3	64.3	131.1	NaN	46.5	46.5	142.8	26.3	-18.8						
MNGE (%)	5.1	6.2	29.6	131.5	101.3	48.6	74.5	134.8	NaN	74.9	74.9	161.2	26.3	22.1						

<sup>a</sup>WS10 and WD10 – Wind speed and direction at 10-m, T2 and RH2 – temperature and relative humidity at 2-m, PBLH – PBL height, TOR – Tropospheric Ozone Residual, Du – Dobson Unit, AOD – Aerosol Optical Depth, corr – correlation, MB – Mean Bias, RMSE – Root Mean Square Error, NMB – Normalized Mean Bias, NME – Normalized Mean Error, MNB – Mean Normalized Bias, and MNGE – Mean Normalized Gross Error.

<sup>b</sup>Observed RH value at one site on one day was zero, which caused infinite values for MNB/MNGE, since this data is 1 of 346 and does not represent the overall trend of the observations at 93 sites, it is excluded for MNB/MNGE calculation.

<sup>c</sup>Observed precipitation values at many sites on many days are zero (346 of 366), these data represent the overall trend of the observations and are included in the statistical calculation. They lead to infinite values for MNB/MNGE (i.e., NaN).

~40.3 and ~50.5 miles southeast of Houston. CMAS56, HALC, BAYP, HOEA, and DRPA represent urban/suburban sites, CONR and C35C represent rural sites, H08H and TLMC represent coastal sites in the Galveston Bay, and GALC is located in the Galveston Island on the Gulf Coast. The model captures well the diurnal variations of the wind at most sites. It reproduces well the observed sea breezes at most sites (e.g., HALC, BAYP, HOEA, C35C, DRPA, H08H, TLMC, and GALC) on August 29 and at TLMC and GALC on August 30–31, although it fails on some days at some sites (e.g., HALC, BAYP, HOEA, C35C, DRPA and H08H on August 30 and 31) and gives higher wind speeds than observations (e.g., TLMC). Table 2 shows overall domain-wide performance statistics. On average, wind speeds at 31 sites are overpredicted by 0.3 m s<sup>-1</sup> (or 11.6%) at the TCEQ sites and -2.4 m s<sup>-1</sup> (or -43.9%) at the NCDC sites. Mean observed wind direction is south-southwesterly while the simulated wind is biased to be more westerly by 20.5 degrees. The nighttime wind biases are larger than daytime (e.g., an NMB of 44.9% versus -9.4% at the TCEQ sites), due likely to the well-known deficiency of meteorological models in accurately simulating nocturnal turbulent mixing near the surface [Bao *et al.*, 2005].

[15] Figures 4 and 5 show the temporal variations of T2 at the above 10 sites and RH2 at 6 sites (i.e., HALC, CAMS56, BAYP, C35C, GALC, DRPA). The model captures well the diurnal variation of T2 at most sites, but tends to overpredict nighttime temperatures at some sites on some days (e.g., CMAS56, BAYP, H08H). It also gives much weaker diurnal variations than the observations at GALC and TLMC, partially because of the model’s incapability in capturing the small scale land-sea circulations and the mismatching of land use and land mask at these sites, i.e., having a land mark of 2 (ocean) instead of 1 (land) in the simulation. Domainwide T2 at 32 sites shows a high correlation of 0.9 and is overpredicted by 0.5°C (with an NMB of 1.7%) at the TCEQ sites but a low correlation of 0.5 and is overpredicted by 1.1°C (with an NMB of 3.5%) at the NCDC sites. While the model captures the diurnal variation of RH2, it tends to underpredict RH2 at the TCEQ sites with a domainwide MB of -18.3% and an NMB of -29.2% but overpredict RH2 at the NCDC sites with a domainwide MB of 5.7% and an NMB of 16%. Large MNB and MNGE values (120.1% and 131.5%, respectively) occur for RH2 at the NCDC sites, due to division of small observed values in calculating MNB and MNGE. For daily precipitation, the NMB and NME values are 15.2% and 210.5%. The observations contain many zero values whereas the simulated values are not always zero, which leads to infinite MNB and MNGE and also a very poor correlation between observed and simulated Precip.

[16] Figure 6 shows the temporal variation of observed and simulated PBLH at 5 sites (i.e., Wharton (WHAR), Ellington Field (ELLF), Southwest Houston (HSWH), Liberty (LBTY), and LaMarque (LMRQ)) around Houston. While the model is able to capture the daytime development and the growth of the PBLH at most sites on most days, it significantly overpredicts the daytime PBLHs (except at LMRQ on August 29) with an NMB of 70.9%. Different methods in determining PBLHs used in observations and the PBL schemes may cause the discrepancies to some extent [Seibert *et al.*, 2000; Fast *et al.*, 2006]. The YSU PBL scheme used in WRF/Chem defines the PBLH as the level at which

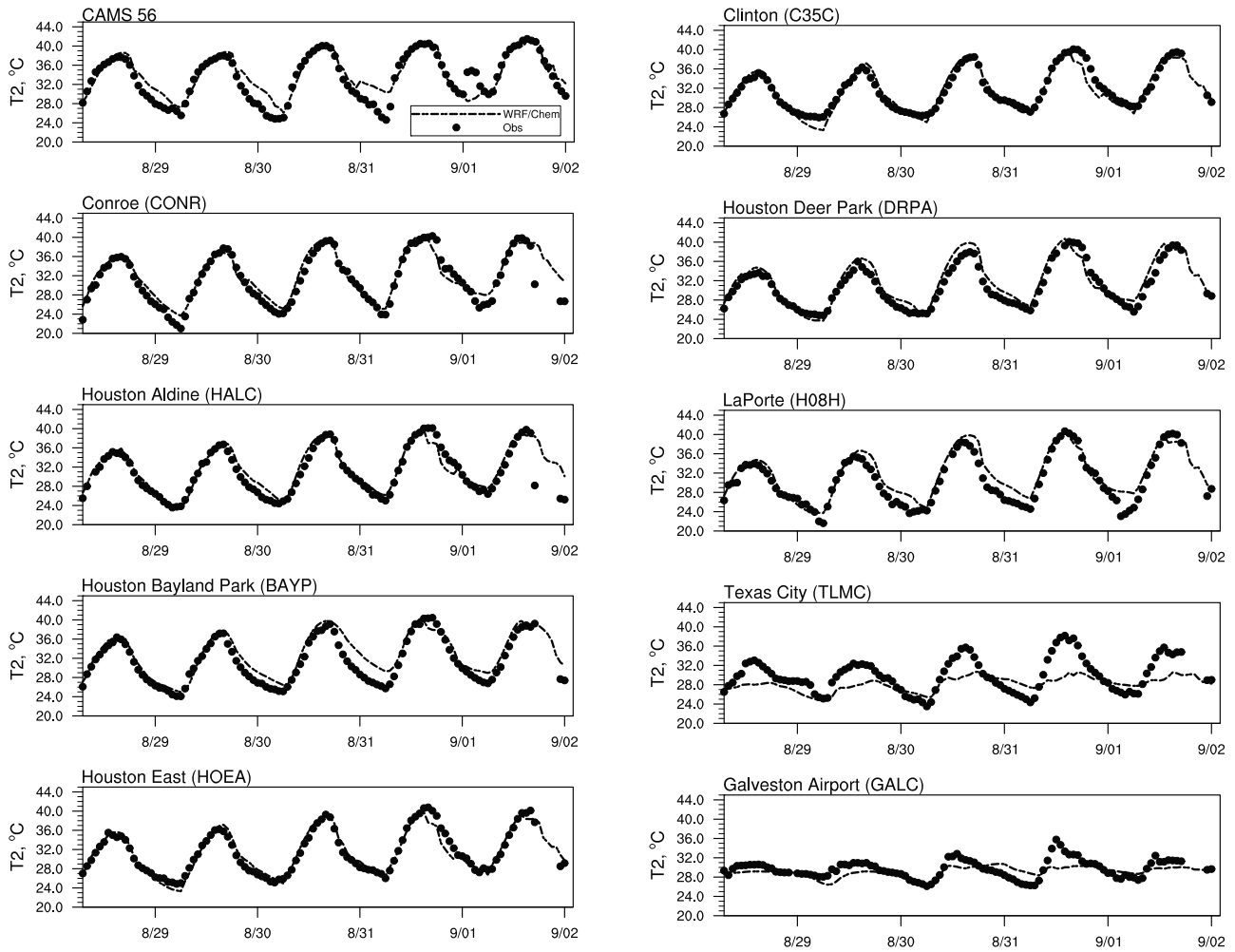


**Figure 4.** Observed and simulated temporal variations of temperatures at two meters (T2) at 10 sites. The simulated results are from the baseline simulation using WRF/Chem-MADRID (EQU).

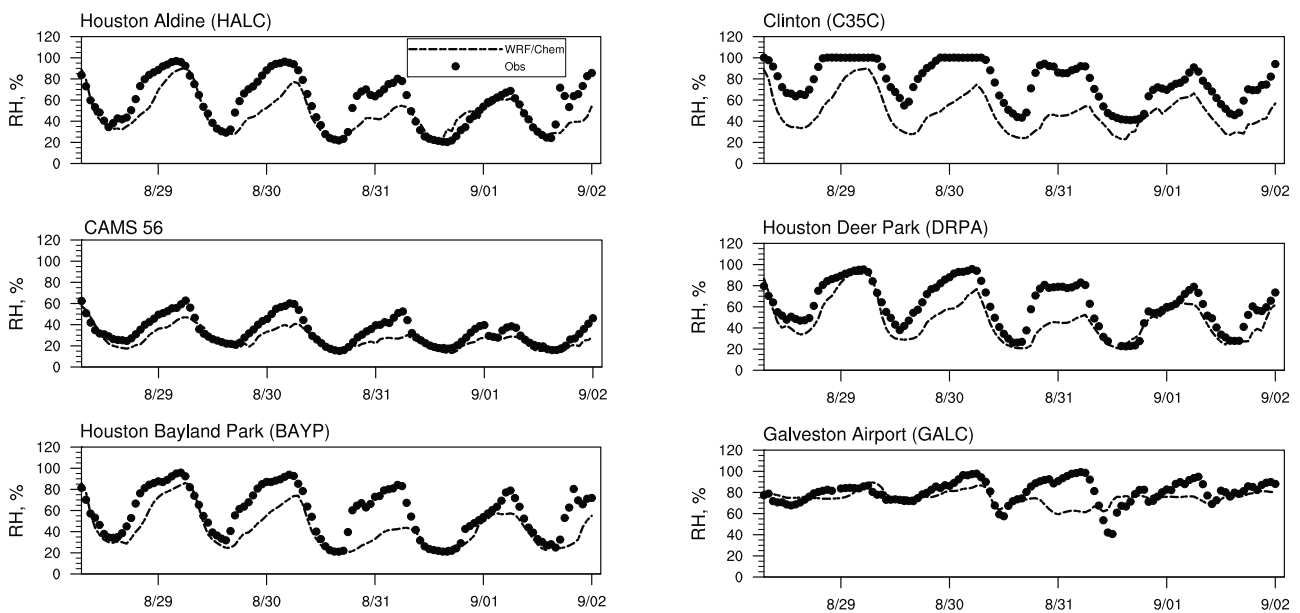


**Figure 5.** Observed and simulated temporal variations of relative humidity at two meters (RH2) at 6 sites. The simulated results are from WRF/Chem-MADRID (EQU).

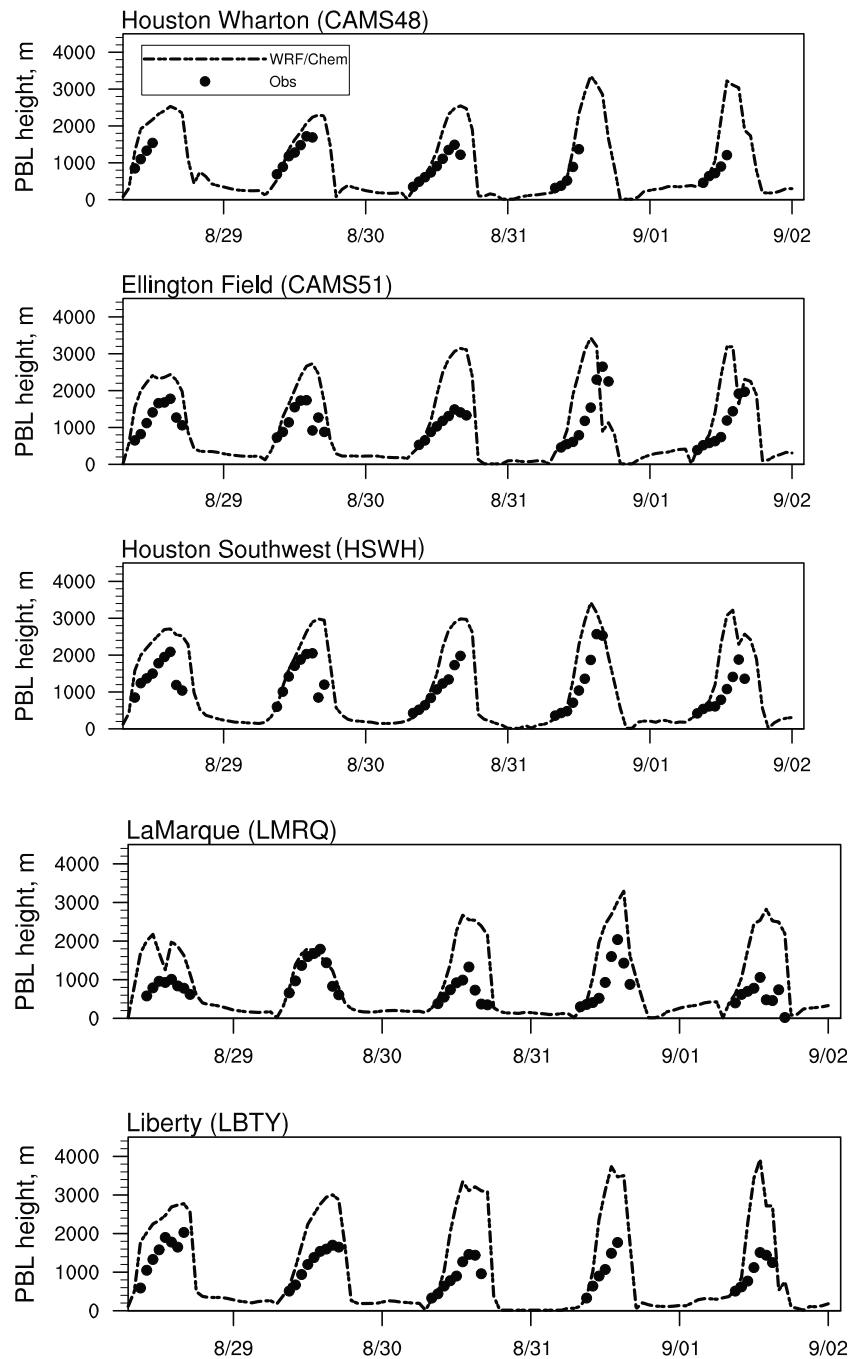


**Figure 6.** Observed and simulated temporal variations of PBL height at 5 sites. The simulated results are from WRF/Chem-MADRID (EQU1).

minimum flux exists (numerically judged by a zero critical bulk Richardson number) [Hong *et al.*, 2006]. The observed PBLHs are derived from the signal-to-noise ratio measured by radar wind profilers [Fast *et al.*, 2006], which may not provide the best estimation (usually biased low) because vertical profiles of winds are more affected by atmospheric dynamics than PBL mixing [Fast *et al.*, 2006]. PBLH at a site in Houston for the same episode was also overpredicted by MM5/Chem [Bao *et al.*, 2005], in which the biases of PBLH were attributed to the errors of grid resolvable model state (wind, temperature, and moisture), the parameteriza-

tions of surface-layer fluxes, soil thermal processes and turbulent mixing within the PBL.

[17] In addition to the evaluation of surface meteorological predictions, the simulated vertical profiles of temperature and RH are also evaluated against the observed profiles below 4 km from the NOAA/NCAR Electra aircraft on August 28, 30, and September 1 along with the flight tracks, as shown in Figure 7. Overall the model reproduces the observed temperature lapse rates, but it fails to capture the observed inversion layers between PBL and free troposphere on August 30 and September 1 due to the imperfect PBL scheme

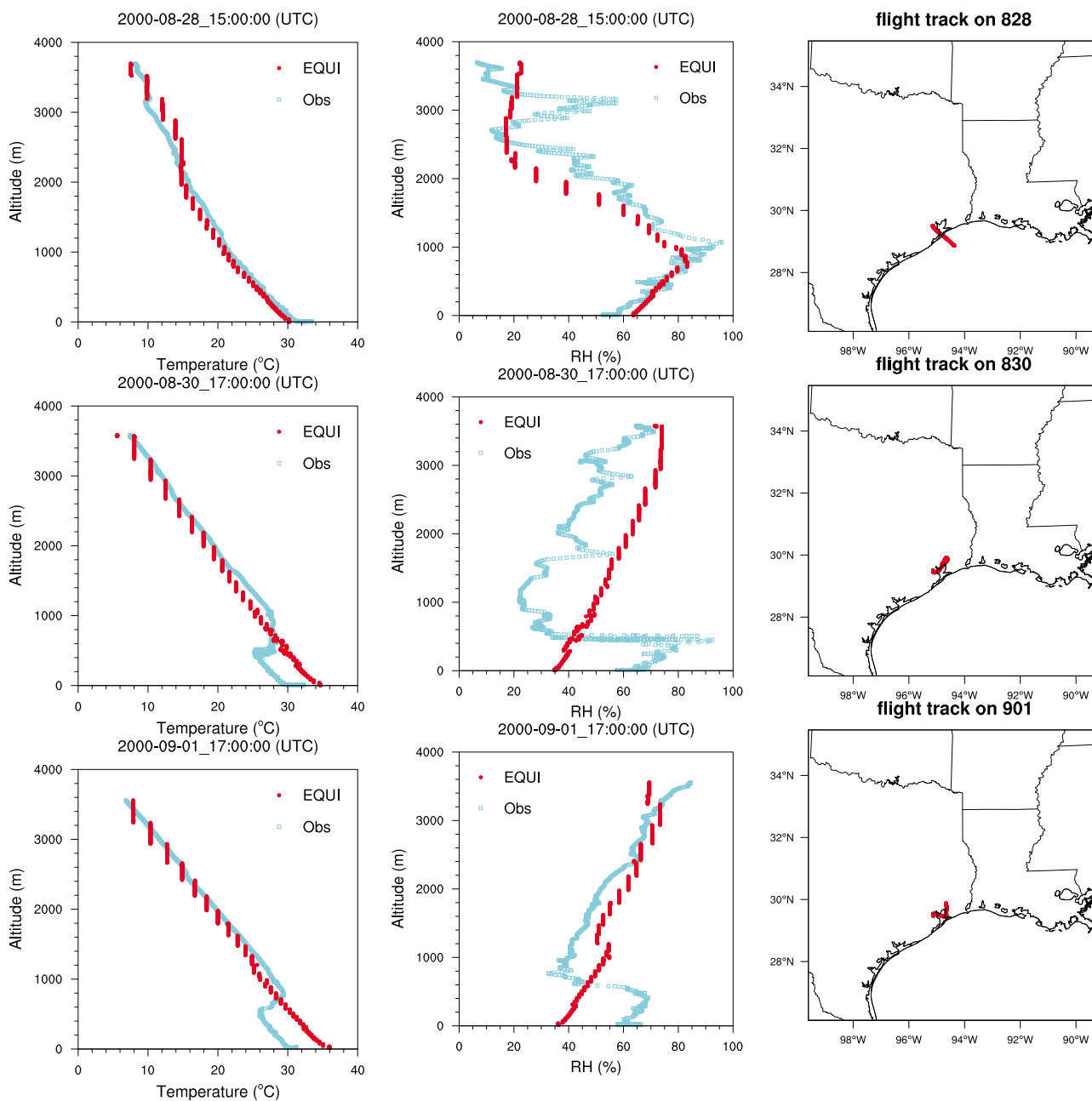


**Figure 7.** Comparison of simulated and observed vertical profiles of temperature and relative humidity and corresponding flight tracks of the NOAA/NCAR Electra aircraft. The simulated results are from WRF/Chem-MADRID (EQUI).

and land-surface module used. The simulated RH profile matches reasonably well with observations on August 28 below 2800 m and those above 1200 m on September 1 but poorly at all heights on August 30. *Misenis and Zhang* [2010] examined the sensitivity of WRF/Chem model predictions to various PBL schemes and land-surface modules in WRF/Chem and found that the vertical profiles of temperature and RH are very sensitive to different schemes.

### 3.2. Chemical Predictions

#### 3.2.1. Surface O<sub>3</sub> Predictions

[18] The evaluation of simulated O<sub>3</sub> mixing ratios focuses on the peak 1-h O<sub>3</sub> values because of frequent exceedances

of the max 1-h O<sub>3</sub> NAAQS during summer 2000. Figure 8 shows the spatial distributions of daily maximum 1-h O<sub>3</sub> mixing ratios from EQUI and observations from TCEQ, AIRS, and CASTNET. High O<sub>3</sub> mixing ratios occurred at a cluster of sites around Houston and a few sites near the border between TX and Louisiana (LA) and in LA on all four days. The observed high O<sub>3</sub> plumes originated from the Houston Ship Channel due to extremely high VOCs (e.g., observed formaldehyde (HCHO) mixing ratio was as high as 25 ppb in the Ship Channel whereas they are generally less than 5 ppb in downtown Houston or its vicinity) [Daum *et al.*, 2003]. During late afternoons and early evenings, a sea breeze brought accumulated O<sub>3</sub> and precursors from the

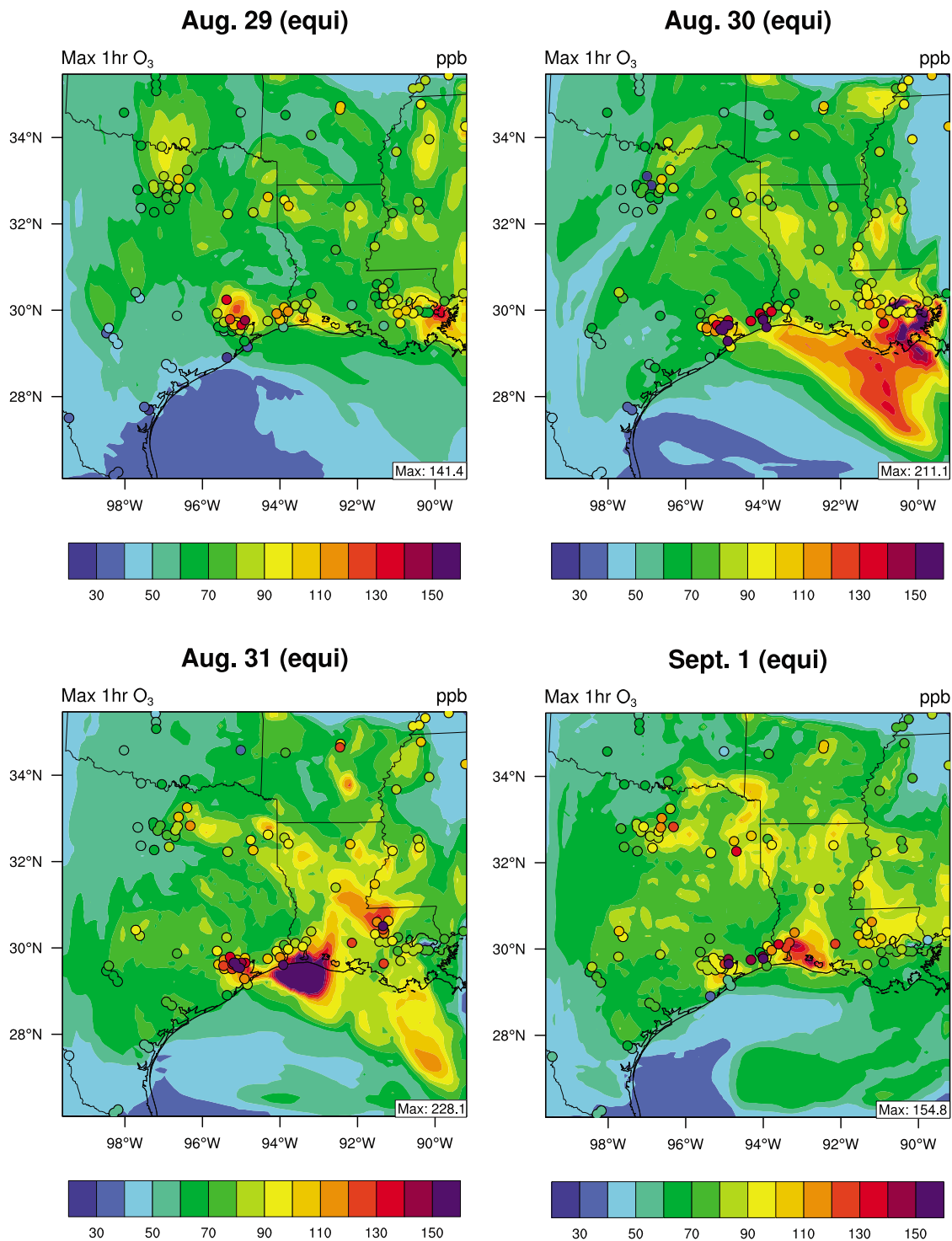


**Figure 8.** Overlay of observed and predicted max 1-h O<sub>3</sub> spatial distributions. The observed max 1-h O<sub>3</sub> values are indicated by the colored dots. The simulation results are based on WRF/Chem-MADRID (EQUI).

Ship Channel to the east side of Houston, leading to the exceedance of the maximum 1-h O<sub>3</sub> NAAQS. The domain-wide NMB for predicted hourly O<sub>3</sub> mixing ratios is 1.4% from EQUI (see Table 2), with NMBs of -1.7% and 10.9% for daytime and nighttime O<sub>3</sub> mixing ratios, respectively, indicating that the model captures O<sub>3</sub> formation better during daytime than at night. During nighttime the predicted hourly

O<sub>3</sub> mixing ratio is biased high by 2.3 ppb which may be due to several possible factors such as an insufficient titration by NO resulted from underestimated NO emissions or a simulated nocturnal PBLH that is not sufficiently shallow. Figure 9 shows the observed and simulated hourly O<sub>3</sub> mixing ratios at 16 out of a total of 60 TCEQ sites: C56 and C401 from the Dallas-Fort Worth area, C59 from the San Antonio

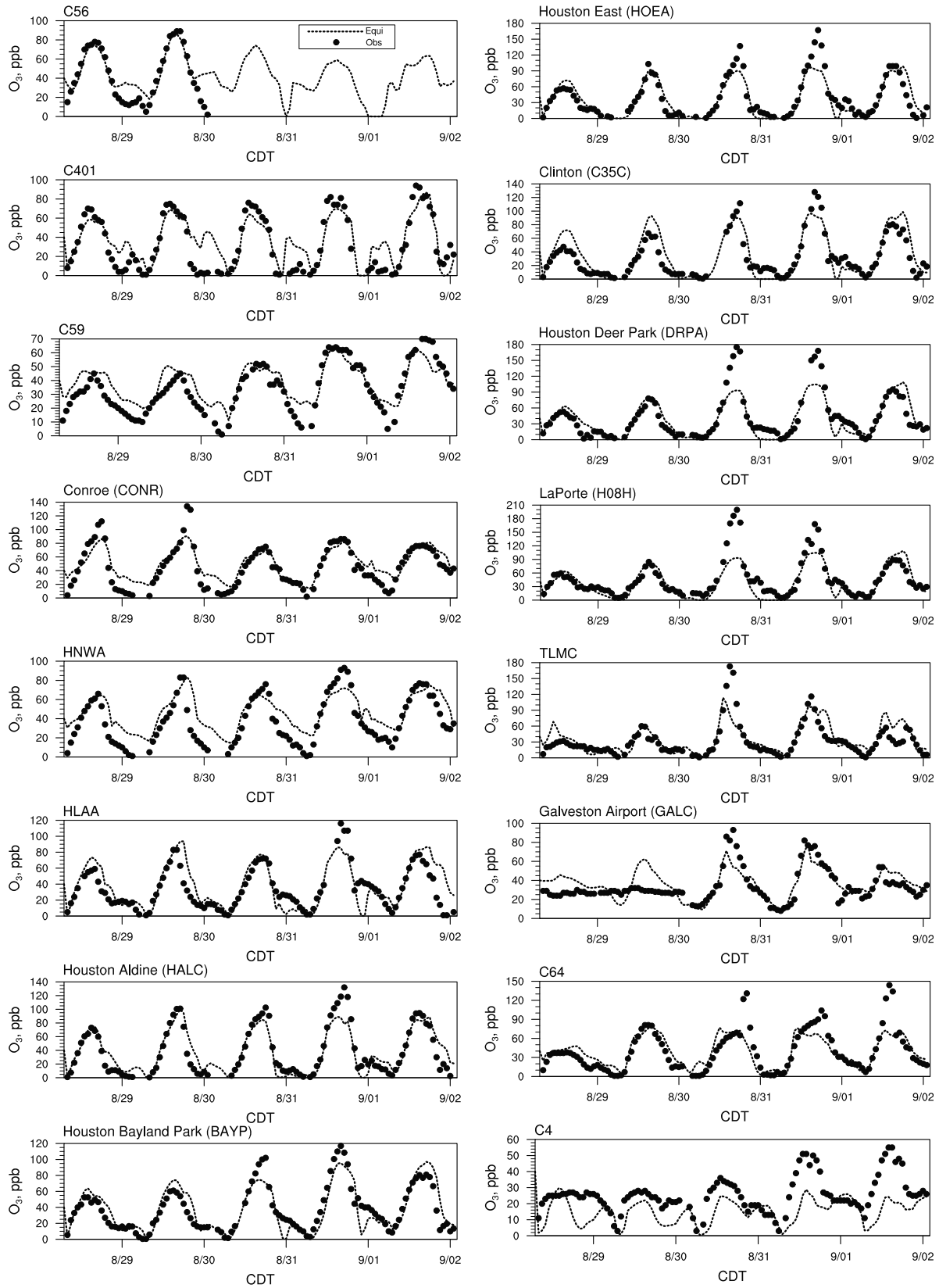


**Figure 9.** Observed and simulated temporal variations of  $O_3$  mixing ratios at 16 sites in TX. The simulation results are based on WRF/Chem-MADRID (EQUI).

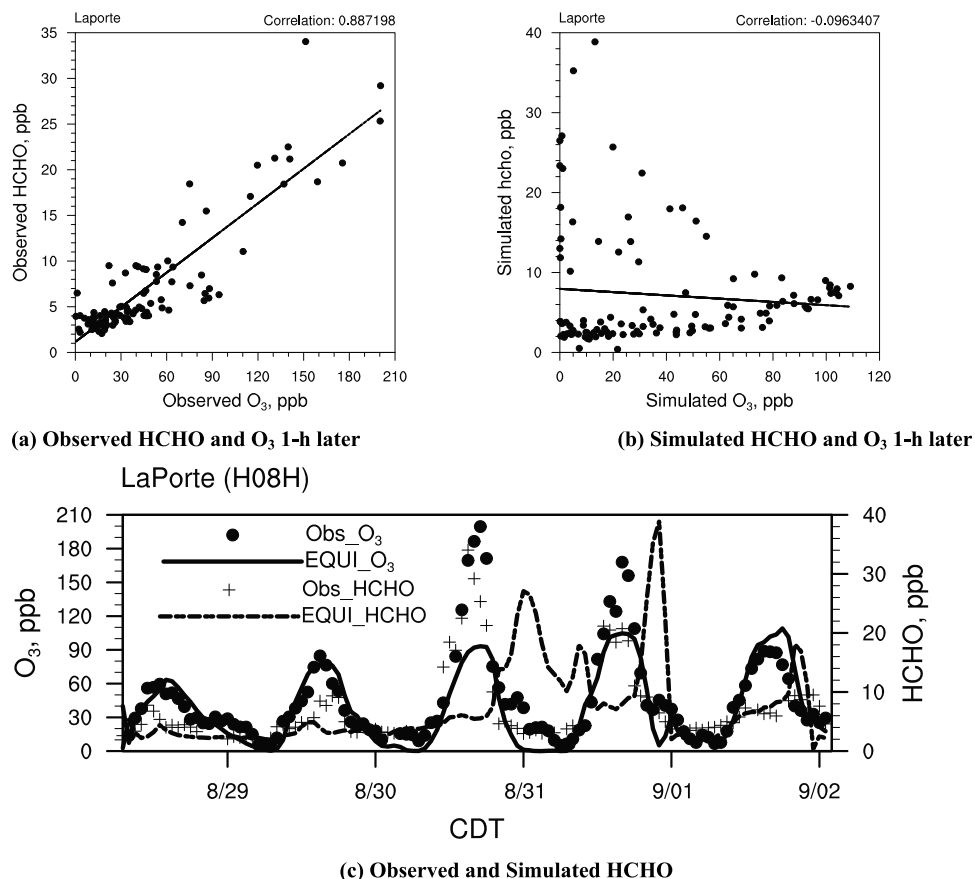


**Figure 10.** Mixing ratios of HCHO and O<sub>3</sub> at LaPorte, TX, (a) correlation between observed HCHO and O<sub>3</sub> 1-h later, (b) correlation between simulated HCHO and O<sub>3</sub> 1-h later, and (c) temporal variation of observed and simulated mixing ratios of HCHO and O<sub>3</sub>. The simulation results are based on WRF/Chem-MADRID (EQUI).

area, CONR, HALC, Houston Northwest Harris Co. (HNWA), Lang C408 (HLAA) from the northwest of Houston, BAYP from the west of Houston, HOEA, C35C, and DRPA from Houston, H08H from the east of Houston, TLMC and GALC from the southeast of Houston, C64 from Beaumont, and C4 from Corpus Christi. The model captures the diurnal variations and magnitudes of surface O<sub>3</sub> mixing ratios quite well at most sites; it tends to overpredict nighttime O<sub>3</sub> mixing ratios at several sites including C56, C401, C59, CONR, and HNWA for the aforementioned reasons and underpredict both daytime and nighttime O<sub>3</sub> mixing ratios at C4 due likely to a lack of local sources in the emissions used. The model significantly underpredicts some observed peak O<sub>3</sub> values at some sites in/near Houston, e.g., 133 ppb on August 31 at HALC, 137 ppb on August 30 and 167 ppb on August 31 at HOEA, 175 ppb on August 30, and 168 ppb on August 31 at DRPA, 199 ppb on August 30 and 167 ppb on August 31 at H08H. These severe O<sub>3</sub> exceedance events have been previously investigated and the industry-emitted ethene and propene could explain the unique O<sub>3</sub> characteristic in Houston [e.g., Kleinman *et al.*, 2002; Ryerson *et al.*, 2003; Wert *et al.*, 2003; Daum *et al.*, 2003; Karl *et al.*, 2003]. Most exceedances resulted from substantial and rapid O<sub>3</sub> production in a single day, which is a unique characteristic of the O<sub>3</sub> problem in Houston, while

in other U.S. cities the highest O<sub>3</sub> mixing ratios generally result from a slower accumulation of O<sub>3</sub> over several days [Ryerson *et al.*, 2003].

[19] Several possible factors may contribute to the model's failure of capturing the observed peak O<sub>3</sub> values at some sites (e.g., HALC, DRPA, BAYP, C35C, H08H) over the Houston-Galveston area. First, the emissions of light olefins (e.g., ethene, propene) are underestimated and their episodic hourly variations may not be accurately represented in the emission inventories [Wert *et al.*, 2003; Ryerson *et al.*, 2003; Jiang and Fast, 2004]. The oxidation of light olefins produces HCHO, an important precursor of O<sub>3</sub>. As indicated by Zhang *et al.* [2009], O<sub>3</sub> chemistry in Houston region is VOC-limited during summer conditions, i.e., high mixing ratios of VOCs will result in high O<sub>3</sub> mixing ratios. HCHO and O<sub>3</sub> measurements are analyzed in Figure 10 along with simulated values at LaPorte (H08H), a coastal site located next to the Houston Ship Channel and affected by the petrochemically produced plumes which produce much higher HCHO mixing ratios than mobile sources and power plant plumes [Wert *et al.*, 2003]. Considering the formation of O<sub>3</sub> may lag behind the emission/formation of HCHO, a 1-h lag correlation is shown between observed HCHO and O<sub>3</sub> mixing ratios and between simulated HCHO and O<sub>3</sub> mixing ratios (i.e., HCHO versus O<sub>3</sub> at 1-h later). The

correlation coefficient is 0.89 between observed HCHO and O<sub>3</sub> at 1-h later, indicating that HCHO-involved reactions play a critical role in O<sub>3</sub> formation at LaPorte during this episode. A high correlation between observed HCHO and O<sub>3</sub> mixing ratios is also found at other in situ sites during TexAQS2000 in the Houston area [Wert *et al.*, 2003]. For example, a plume of very high olefin (>100 ppb) emitted from around 2.5 km north of DRPA at around 10:40 A.M. on August 30, 2000 was detected by a NOAA aircraft [Vizuete, 2005]. Giving the northwesterly wind around this time, some downwind sites, e.g., DRPA and LaPorte (H08H) (~7.5 km southeast to DRPA), were affected by this emission event. High O<sub>3</sub> mixing ratios were observed at DRPA and H08H on August 30. The simulated mixing ratios of HCHO and O<sub>3</sub> at 1-h later, however, are poorly correlated (with a correlation coefficient is -0.1). As shown in Figure 10c, the hourly mixing ratios of HCHO peak during late night on August 31 and early morning on September 1 (rather than mid-to-late afternoons when the O<sub>3</sub> formation rate is the highest). The misalignment of peak mixing ratios of HCHO emitted or produced via chemical reactions, resulted from incorrect hourly HCHO and its precursors' emission profiles (not shown), as well as the VOC-limited O<sub>3</sub> chemistry in this region, explain in part the failure of the model in capturing the peak O<sub>3</sub> on both days as shown in Figure 9. Second, intense wildfire emissions of NO<sub>x</sub>, CO, and VOCs during this time period reported by Junquera *et al.* [2005] were not represented in the emissions used. Third, meteorological conditions are not accurately captured, in particular, the overpredictions in the daytime PBLH and sea/bay breezes. For example, the observed wind changes during sea/bay breezes from northwesterly to southerly at HAEL, HOEA, DRPA, and H08H on August 30 and 31 are not well captured by the model due to the lack of penetration of simulated sea breeze (see Figure 3), which is believed to partially cause O<sub>3</sub> bias on this day. Four, a coarse grid resolution of 12-km may also be responsible for the model's failure in reproducing the peak O<sub>3</sub> mixing ratios due to a use of grid-averaged emissions and concentrations that often cannot well resolve their small-scale gradients needed to reproduce point-wise peak O<sub>3</sub> mixing ratios. Finally, missing gas-phase reactions in the model may also contribute to the underestimation of peak O<sub>3</sub> mixing ratios on some days at some sites. For example, recent research has shown that chlorine radical chemistry has the potential to enhance O<sub>3</sub> formation [Chang *et al.*, 2002; Tanaka *et al.*, 2003; Chang and Allen, 2006; Sarwar *et al.*, 2008]. Simulated peak 1-h O<sub>3</sub> mixing ratios around the Houston area during TexAQS-2000 may be lowered by 5 ppb if chlorine chemistry were excluded [Chang and Allen, 2006], implying that neglecting chlorine chemistry in the CBM-Z gas phase mechanism may have contributed to the underprediction in peak O<sub>3</sub> values.

### 3.2.2. Surface PM<sub>2.5</sub> Predictions

[20] Annual mean PM<sub>2.5</sub> concentration in the southeastern TX is close to the NAAQS of 15 μg m<sup>-3</sup> and tends to be higher near urban and industrial areas of Houston [Russell *et al.*, 2004]. Observed daily average PM<sub>2.5</sub> concentrations are overlaid with the predictions from EQUI, HYBR, and KINE in Figure 11. EQUI simulates well the observed concentrations in the north and west of the domain on August 30–31, and most of the domain on September 1, but tends to overpredict PM<sub>2.5</sub> concentrations over the down-

town Houston and its vicinity on August 29–31. As shown in Table 2, EQUI overpredicts surface PM<sub>2.5</sub> by 26.4% in terms of NMB. The values of NME, MNB, and MNGE are 59.9%, 142.8%, and 161.2%, respectively. Large values of MNB, and MNGE are caused by division of small observed values in their calculation, which do not occur for the calculation of NMB/NME. The background PM<sub>2.5</sub> values of 8 μg m<sup>-3</sup> used in the simulation may be too high, partially responsible for the overprediction in PM<sub>2.5</sub> concentrations at night [Fast *et al.*, 2006]. Other uncertainties include possible overestimation in primary PM<sub>2.5</sub> emissions, in particular, the emissions of other inorganic aerosols (OIN) and inaccuracy in simulated meteorology (e.g., shallower nocturnal PBLH than observations), which may result in overpredictions in the concentrations of primary PM<sub>2.5</sub> and the precursors of secondary PM<sub>2.5</sub>. Figure 12 shows the observed and simulated PM<sub>2.5</sub> temporal variations at 15 sites. The hourly observed data were collected with the Rupprecht and Patshnick Partisol Model 2025 Sequential Air Samplers except at two supersites: Williams Tower (WT), where the Tapered Element Oscillating Microbalance (TEOM) samplers were used and LaPorte where the Scanning Mobility Particle Sizer and Aerodynamic Particle Sizer tandem (SMPS-APS) were used. TEOM measured PM<sub>2.5</sub> concentrations may have negative biases due to the evaporation of semi-volatile species as a result of using heating method to remove condensed water during the collection process; in some cases the underestimation may be as high as -50% [Lee *et al.*, 2005]. The model captures reasonably well the temporal variations and/or magnitudes at several sites during most of time (e.g., GALC, WT, CONR, C64, and C302), but large discrepancies exist at some sites during some periods (e.g., at H08H, C66, and C4 on all days, at C301, C94, C401, C56, and C59 on August 28–29, and at HOEA and DRPA on August 30–31), due to the uncertainties in the local emissions of primary PM and the precursors of secondary PM, ICONs and BCONs of PM<sub>2.5</sub>, as well as in the PM<sub>2.5</sub> measurements due to the loss of volatile masses. Unlike O<sub>3</sub> mixing ratio that only has one peak in its daily variation, two peaks in the observed diurnal variation of PM<sub>2.5</sub> concentrations often occur at most sites [Russell *et al.*, 2004], which can be shown clearly and compared with simulated mean diurnal variation of PM<sub>2.5</sub> concentrations in Figure 13. Strong traffic sources, low PBLHs, nitrate formation due to ammonia excesses and low temperatures, and bursts of photochemical activity associated with sunrise may explain the early morning peak [Russell *et al.*, 2004; Pavlovic *et al.*, 2006]. The afternoon peak may reflect a contribution from secondary sources (e.g., from biogenic SOA at CONR [Lemire *et al.*, 2002]) and strong traffic sources, as well as the impact of reduced PBLH.

[21] Figure 14 compares the simulated and observed concentrations of PM<sub>2.5</sub> components at LaPorte (H08H) where the observed speciated PM<sub>2.5</sub> concentrations were measured using the Particle Composition Monitor (PCM). PCM collects PM<sub>2.5</sub> samples on discrete time scales between 6 and 24 h depending on pollution level [Lee *et al.*, 2005]. Note that OIN is not directly measured, which is derived as the difference between measured PM<sub>2.5</sub> and a sum of total mass of other measured species (i.e., sulfate (SO<sub>4</sub><sup>2-</sup>), nitrate (NO<sub>3</sub><sup>-</sup>), ammonium (NH<sub>4</sub><sup>+</sup>), sodium (Na<sup>+</sup>), chloride (Cl<sup>-</sup>), elemental carbon (EC), organic matter (OM)). Thus, the bias of directly measured species may accumulate into the bias

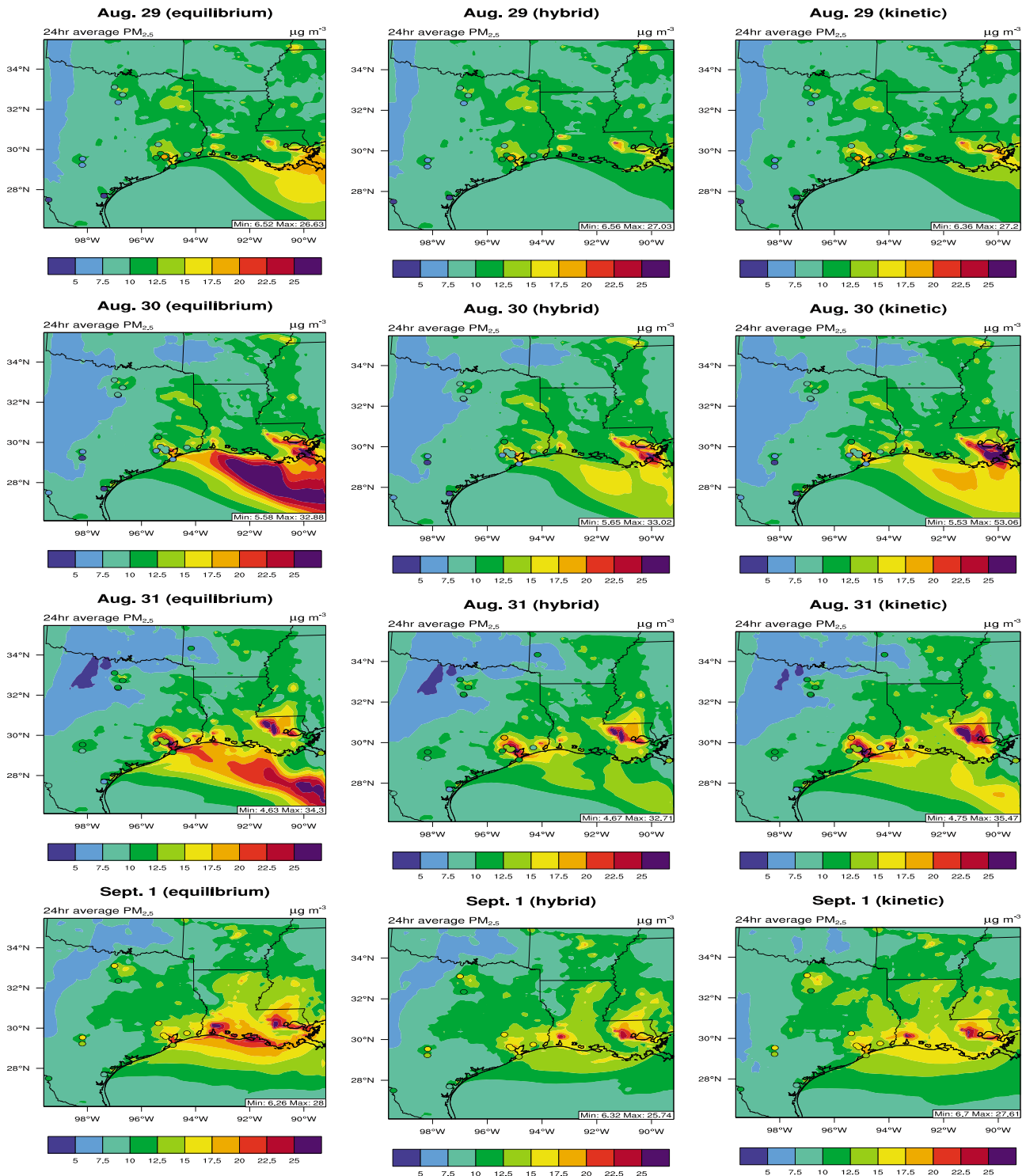


**Figure 11.** Overlay of observed and simulated daily average spatial distributions of PM<sub>2.5</sub> mass concentrations. Observed PM<sub>2.5</sub> concentrations are indicated by the circles.

of OIN. As shown, the model overpredicts total PM<sub>2.5</sub> concentrations significantly on August 30–31 and September 1 at LaPorte mainly due to the overprediction of OIN. The other species concentrations are predicted reasonably well. In addition to the underestimate in the nocturnal PBLH, the overprediction of OIN may be due to uncertainties in its

emissions and improper initial condition. As described in *Fast et al.* [2006], 3.48 out of 8 µg m<sup>-3</sup> is assigned to OIN as initial condition. In addition, 75% of total PM<sub>2.5</sub> emissions used in the simulation are assumed to be OIN, which may be too high. According to *Russell et al.* [2004], on the average, SO<sub>4</sub><sup>2-</sup>, OM, and NH<sub>4</sub><sup>+</sup> are the largest components in the

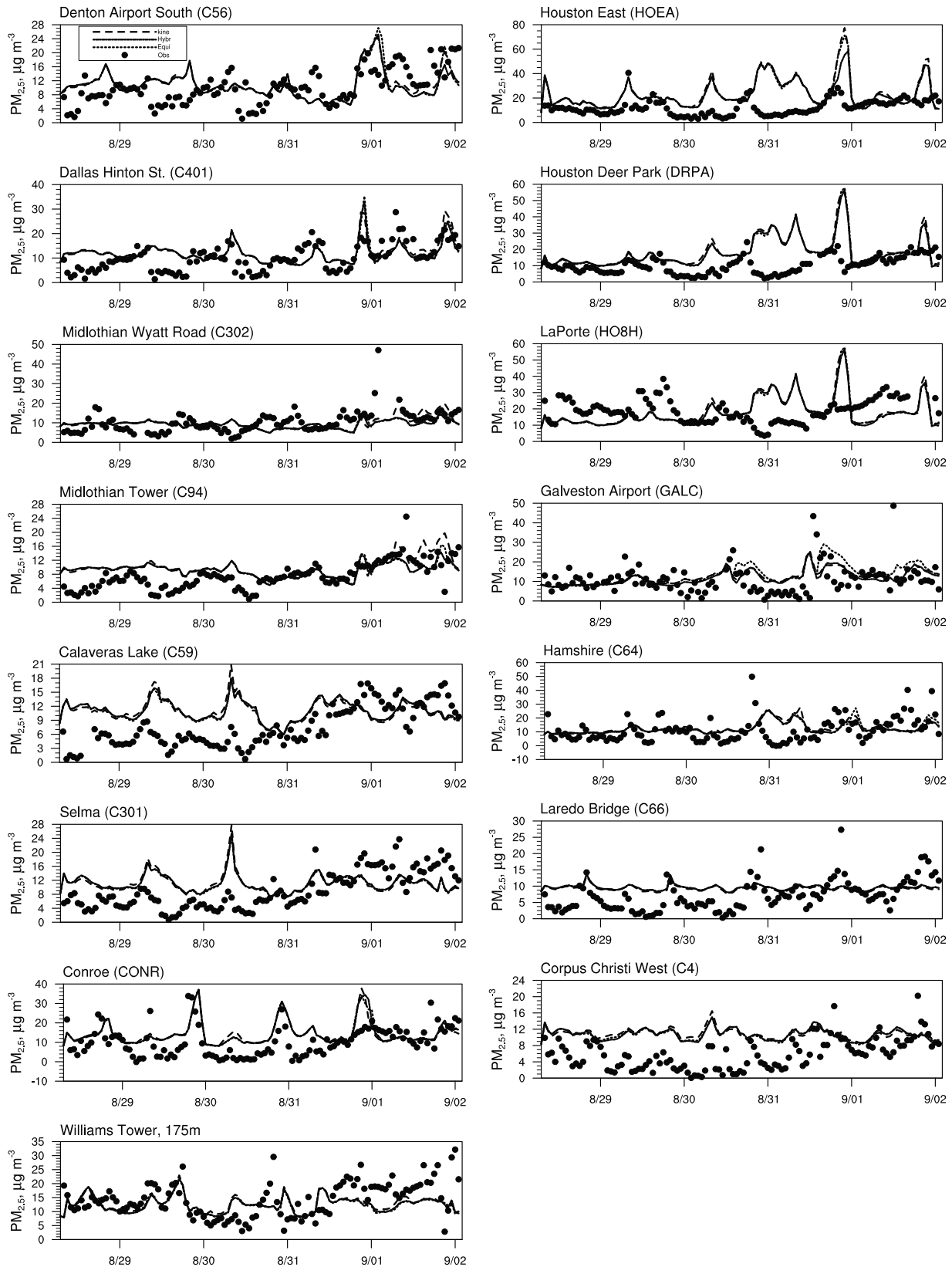
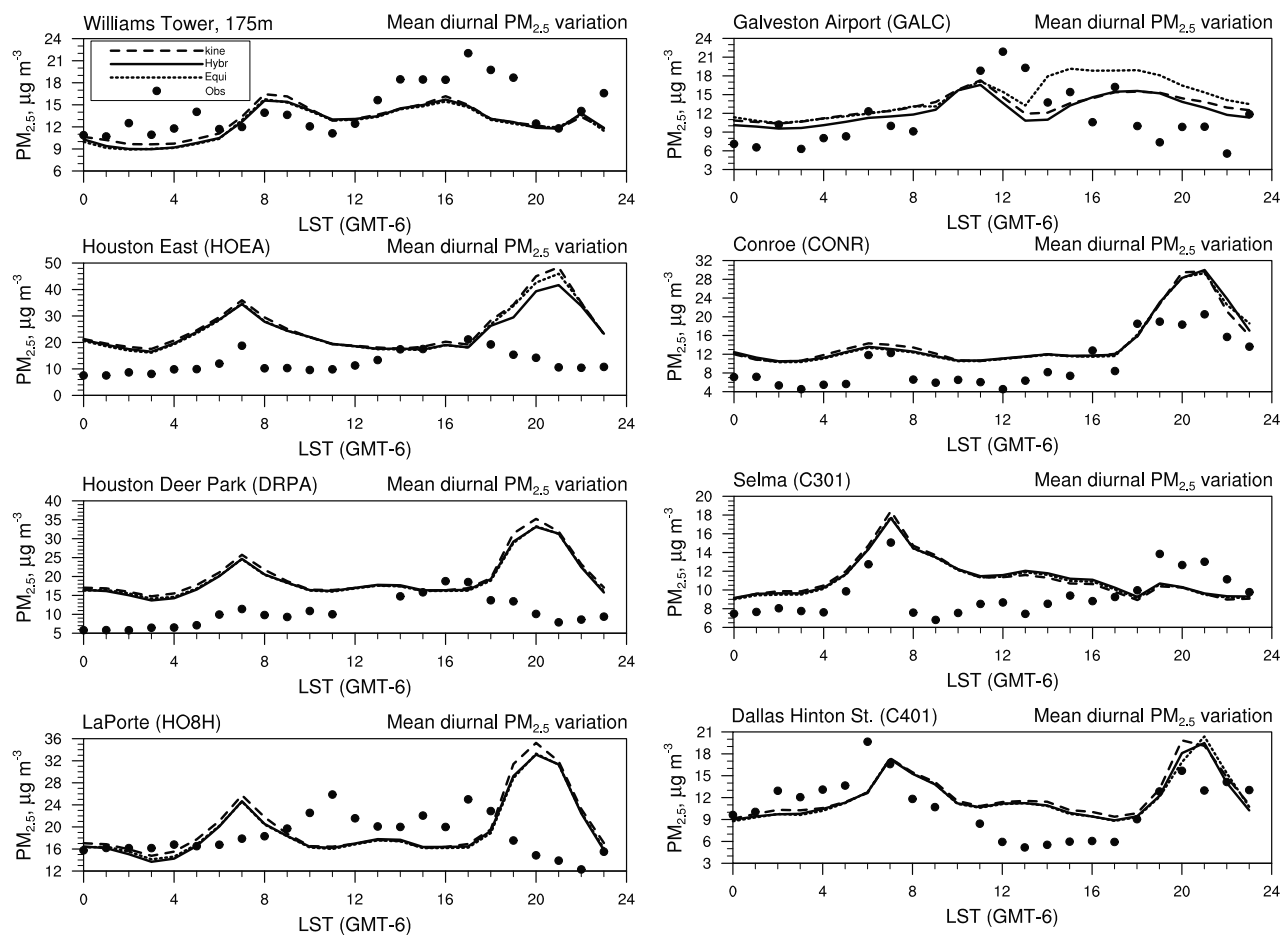


Figure 12. Observed and simulated temporal variations of PM<sub>2.5</sub> concentrations at 15 sites.



**Figure 13.** Mean diurnal pattern of  $PM_{2.5}$  mass concentrations at 8 observational sites.

southeast Texas and account for 32%, 30%, and 9% of total  $PM_{2.5}$ , respectively. Since OIN in  $PM_{2.5}$  is treated to be non-reactive and its removal rate is relatively low (because the deposition rate for  $PM_{2.5}$  is relatively low), the lifetime of OIN in  $PM_{2.5}$  may be longer than what it should be. OM concentrations are overpredicted on August 29 and 31 but underpredicted on August 30 and September 1. OM makes up ~25–30% of total  $PM_{2.5}$ ; primary emissions are its dominant source around the Houston area [Russell and Allen, 2004; Allen and Fraser, 2006]. The discrepancies between simulated and observed OM are therefore most likely due to uncertainties in primary OM emissions (e.g., uncounted wildfire emissions on August 30 and September 1), although a lack of SOA formation may also contribute to the OM underpredictions.

### 3.2.3. Predictions Aloft

[22] The simulated and observed profiles of CO, NO,  $NO_2$ , and  $O_3$  mixing ratios from the NOAA/NCAR Electra aircraft are compared in Figure 15. Overall the model captured reasonably well the observed vertical distributions. However, the observed profiles of all four species peaked at ~1 km above ground on August 28, which are not captured by model simulations. Since the model predicts the meteorological parameters well along the flight track (see Figure 7), indicating that the biases in these vertical profiles may not come from the biases in meteorological predictions. The model underpredicts the observed mixing ratios at ~1 km for

CO and  $NO_x$  on all days, but overpredicts those for  $O_3$  on August 28 and 30, indicating that there may be some local emission events such as wildfires that occurred at this altitude but were not captured by the model. On August 30 and September 1, larger discrepancies occur between simulated and observed chemical profiles in the PBL than in the free troposphere, indicating that the chemical and physical processes in the PBL are more complicated than in free troposphere due largely to the uncertainties of emissions and the current model treatments in PBL processes and land-surface interaction. The observed temperature inversion layer at the top of PBL is not reproduced by the model, which may partially contribute to the biases in chemical predictions. In addition, the vertical profiles of these species are sensitive to various PBL schemes and land-surface modules [Misenis and Zhang, 2010]. In free/upper troposphere, the differences between observed and simulated CO and  $O_3$  profiles on Sept. 1 are larger than those on other days, indicating a larger impact by long range transport on this day. Such differences are caused by the uncertainty in the upper layer boundary conditions for CO and  $O_3$ . For example, boundary conditions for CO are set to be 70 ppb at the top layer and 80 ppb throughout the troposphere for all simulations, which may be lower than what was observed on Sept. 1. A sensitivity simulation is conducted using a CO boundary condition of 120 ppb throughout the troposphere. The results show improved CO mixing ratios aloft [Misenis and Zhang, 2010].

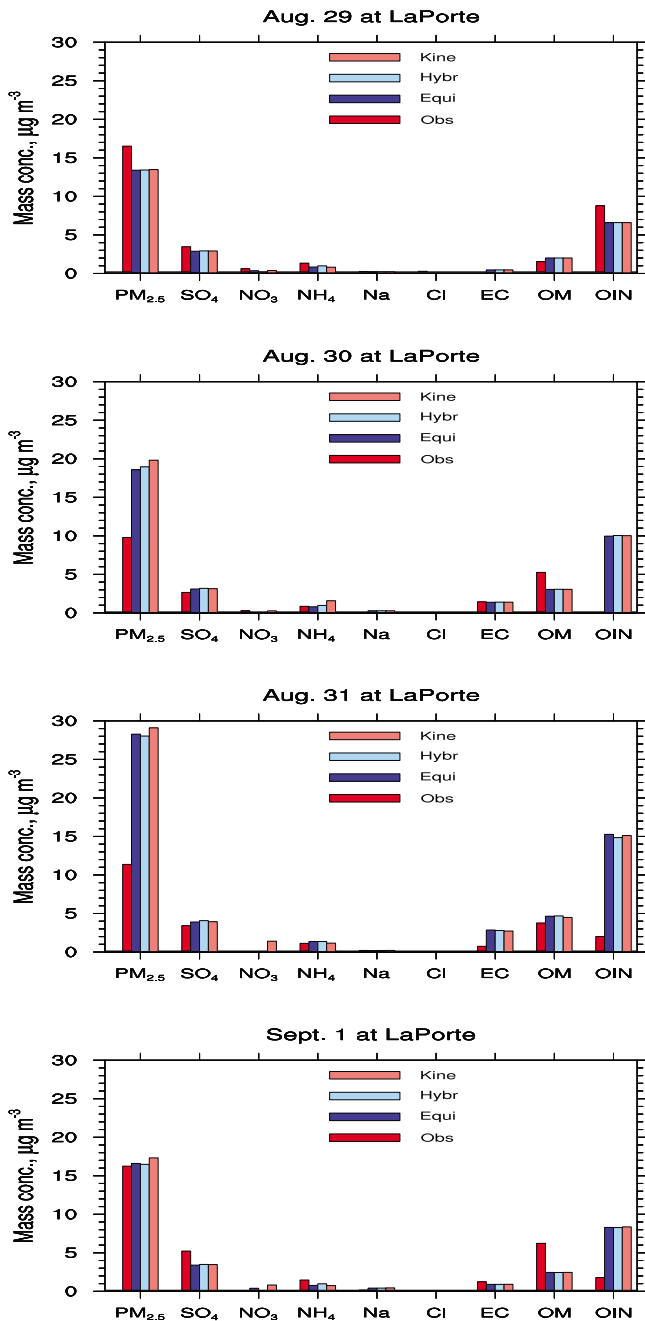


**Figure 14.** The mass concentrations of daily average  $\text{PM}_{2.5}$  and its component at LaPorte, TX.

[23] Figure 16 shows the comparison between simulated and observed TORs from TOMS/SBUV on August 29–September 1, 2000. While the simulated TOR values are within the range of observations, large discrepancies exist in their spatial distributions. In particular, the observed TORs show high values in the northern portion of the domain on August 29 and the eastern portion on the rest of days, whereas the simulated values peak in the southeastern LA on August 29 and in the triangle areas covering Houston, TX, Shreveport, LA, and Lafayette, LA, and a portion of the Gulf of Mexico on August 30–31, and extend northwest into Dallas and Fort Worth areas on September 1. The dis-

agreement in spatial distribution is attributed to a poor representation of  $\text{O}_3$  aloft that is more affected by large scale transport rather than local emissions and chemistry and that dominates TORs. A constant chemical BCON of 168 ppb for the top model layers (for layers with an altitude above 12.1 km or pressure less than 250 mb) is, however, used for  $\text{O}_3$  in WRF/Chem. Zhang *et al.* [2010b] performed simulations over the U.S. using different BCONs for  $\text{O}_3$  in upper layers and found a high sensitivity in simulated TORs.

[24] Figure 17 compares the MODIS-retrieved AODs on August 29 to September 1 with the total column AOD simulated by EQUI. On August 29 and 30, simulated AOD captures the spatial gradient of MODIS-derived AODs, despite underpredictions in the eastern domain. On August 31 and September 1, some discrepancies occur between simulated and observed AODs. The area with high AODs simulated by WRF/Chem on September 1 is mostly over oceanic areas whereas the MODIS AODs show high values along the coast of TX, the southwest corner of Missouri (MO), and most areas in LA. The NMB and the correlation coefficient between the simulated and MODIS-retrieved AODs on August 29–September 1 are  $-23.2\%$  and  $0.75$ , respectively. Several studies reported that MODIS AODs correlate highly with surface  $\text{PM}_{2.5}$  concentrations in the eastern U.S., thus providing a good indicator of  $\text{PM}_{2.5}$  level [e.g., Hutchison *et al.*, 2008]. The accurate derivation of ground-level PM from MODIS may be possible given the detailed aerosol vertical distributions [Chu *et al.*, 2003]. Figure 18 compares observed versus simulated AODs and surface  $\text{PM}_{2.5}$  concentrations at 10:30 A.M. at HEOA, H08H/DRPA, and GALC during August 28–September 1, 2009. While large discrepancies between simulated and observed  $\text{PM}_{2.5}$  concentrations exist, those between simulated and observed AODs are smaller except on August 30 at GALC and on September 1 at HOEA (note that the observed and simulated AODs and simulated  $\text{PM}_{2.5}$  concentrations at H08H and DRPA are the same because they fall into the same 12-km grid cell). At HEOA, while the simulated surface  $\text{PM}_{2.5}$  concentrations are much higher than observations on all days, simulated and observed AODs are much closer during August 28–31. The simulated AODs on August 29 and September 1 are lower than observations, despite higher simulated surface  $\text{PM}_{2.5}$  concentrations, indicating an underestimation in  $\text{PM}_{2.5}$  concentrations aloft. At GALC, a good agreement is found between simulated and observed AODs on August 28, 29, and 31 and between simulated and observed  $\text{PM}_{2.5}$  concentrations on August 28–30 but substantial inconsistencies exist between these values on August 30 and 31. Unlike HOEA and DRPA, simulated  $\text{PM}_{2.5}$  concentrations are much lower than observations except for August 31 at H08H, which has been compensated by  $\text{PM}_{2.5}$  concentrations aloft to some extent to result in a reversed trend between simulated and observed AODs on August 28 and 30. No consistent trend exists between them at H08H, but a more consistent trend can be found at DRPA. The correlation coefficients between observed AODs and  $\text{PM}_{2.5}$  concentrations are  $0.72$ ,  $0.63$ ,  $0.23$ , and  $0.96$  at HOEA, GALC, H08H, and DRPA, respectively, and those between simulated AODs and  $\text{PM}_{2.5}$  concentrations are  $0.61$ ,  $0.48$ ,  $0.83$ , and  $0.83$  at those sites, respectively, indicating a strong spatial/temporal variability in their correlations. Such

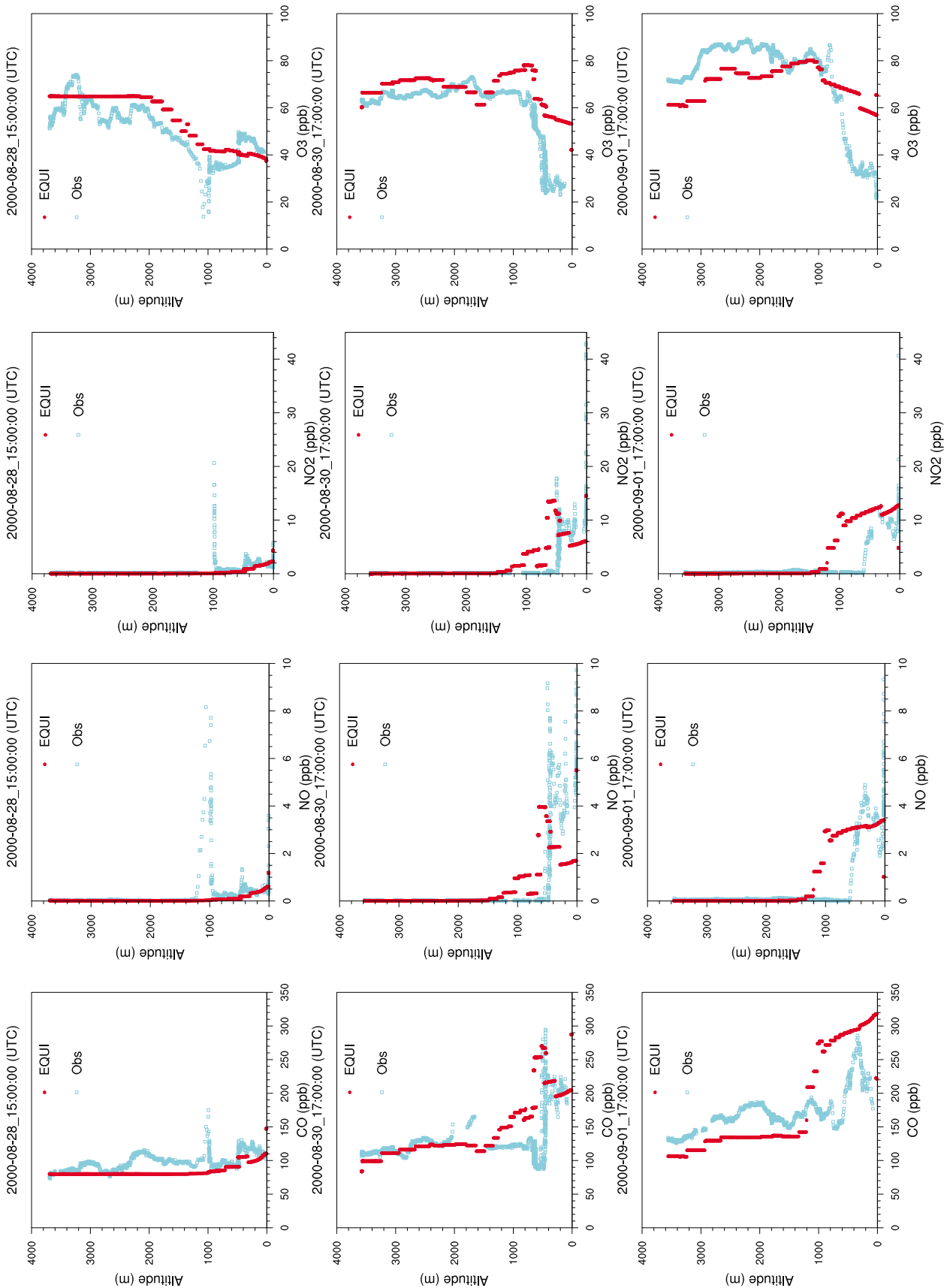


**Figure 15.** Comparison of simulated and observed vertical profiles of chemical species (CO, NO, NO<sub>2</sub>, and O<sub>3</sub>). The simulated results are from WRF/CHEM-MADRID (EQUI).

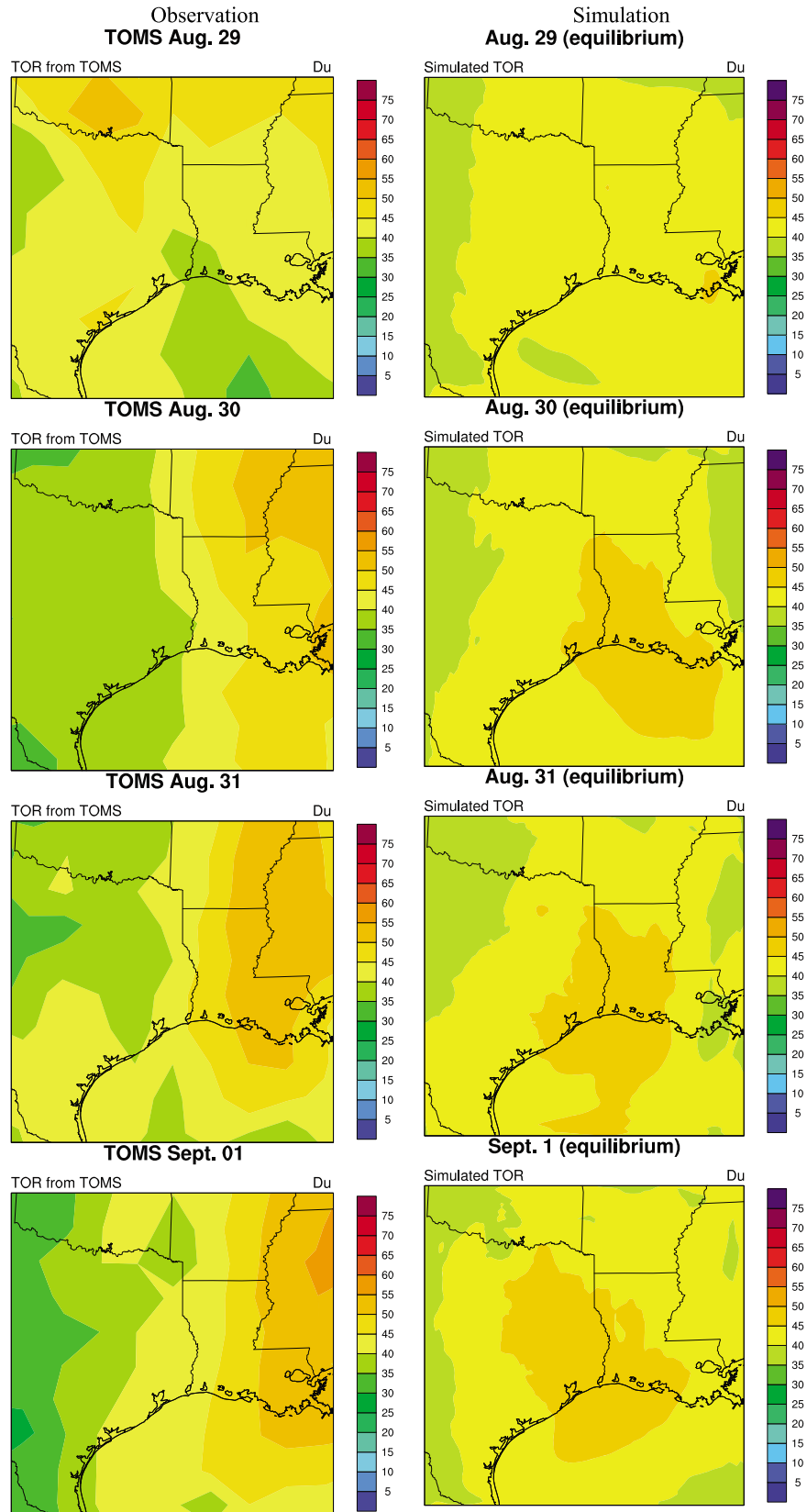


**Figure 16.** Comparison between simulated Tropospheric Ozone Residuals (TOR) and observed TORs from TOMS/SBUV. The simulated results are from WRF/Chem-MADRID (EQU).

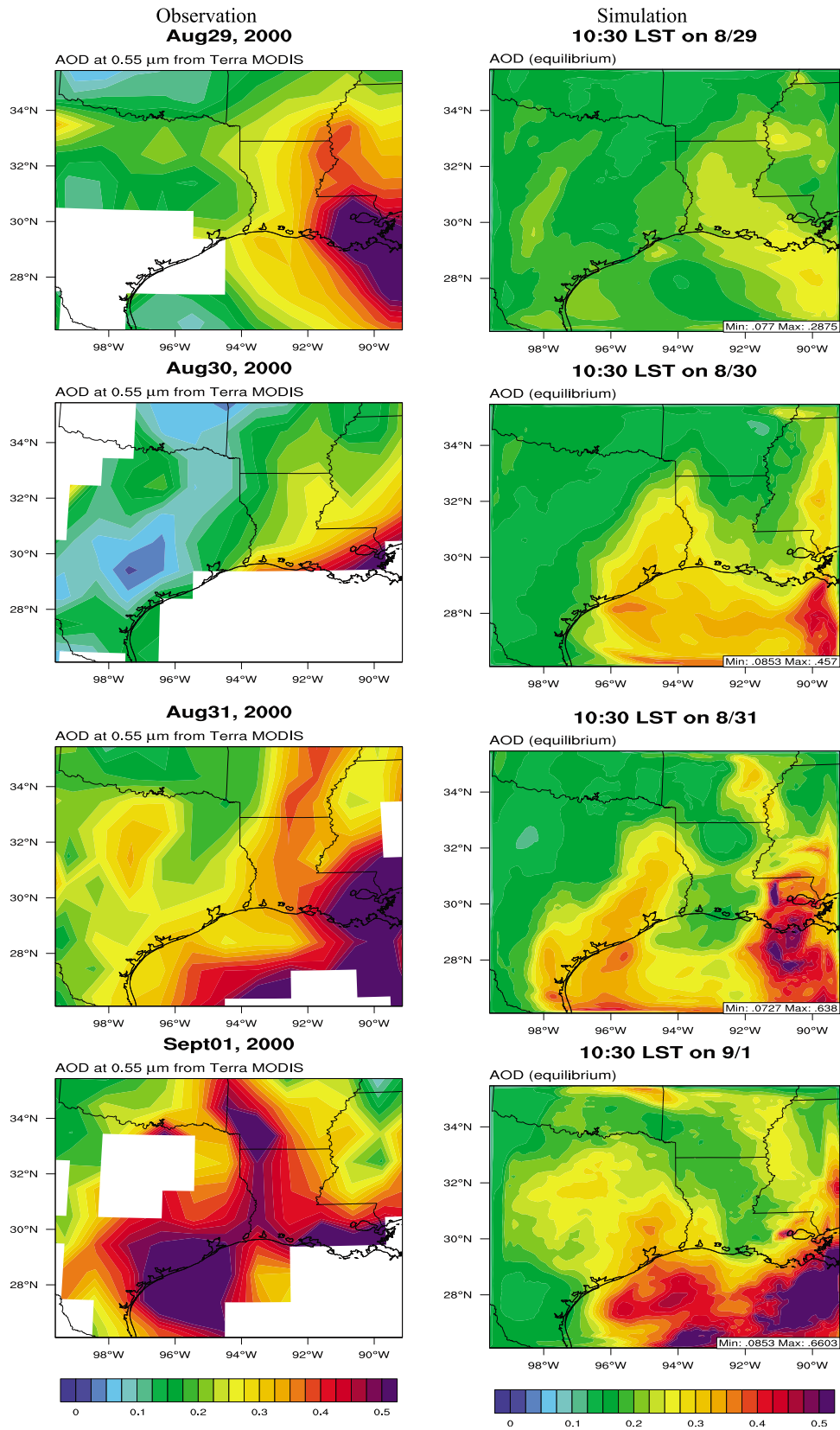


**Figure 17.** MODIS-derived AOD and simulated total column AOD from WRF/Chem-MADRID. The blank areas in the MODIS AOD plots contain no MODIS data. The simulated results are from WRF/Chem-MADRID (EQUI).

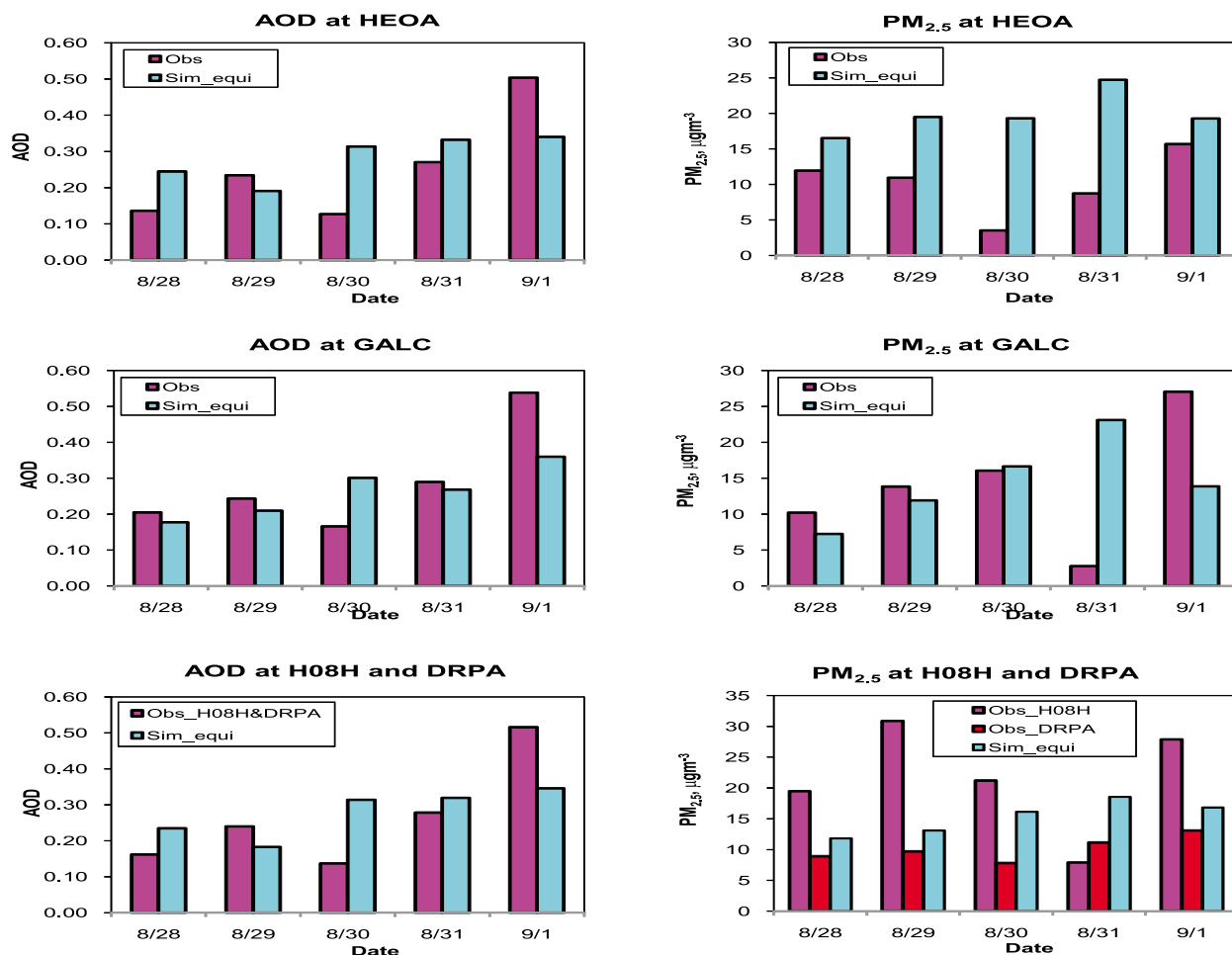


**Figure 18.** Simulated versus observed AODs and PM<sub>2.5</sub> concentrations at HOEA, GALC, H08H, and DRPA. The simulated results are from WRF/Chem-MADRID (EQUI). The observed AODs and PM<sub>2.5</sub> concentrations are based on MODIS and TCEQ measurements. The simulated AODs and PM<sub>2.5</sub> concentrations are the same at H08H and DRPA, because they fall into the same 12-km grid cell in the simulation. The observed AODs at H08H and DRPA are also the same because the MODIS-derived AOD database has a grid resolution of 10-km, and they fall into the same 12-km grid cell that maps the original MODIS AODs into the model simulation domain.

variabilities must be accounted for when using MODIS AODs to indicate surface PM<sub>2.5</sub>.

[25] The discrepancies between observed and simulated AODs are likely due to the biases from both MODIS data and the model. MODIS AODs have bias [Heald *et al.*, 2006] and their retrieval algorithm may need improvements [Levy *et al.*, 2007]. MODIS AODs cannot be retrieved (or have a large uncertainty) under certain conditions such as cloudy, strong sun glint from bodies of water, and over snow/ice and bright desert areas [Al-Saadi *et al.*, 2005]. The bias of simulated AODs is directly associated to the bias of PM vertical profile, which may be attributed to several factors. For example, Junquera *et al.* [2005] reported intense wildfires in the southeast Texas during August and September 2000 that emitted a large amount of CO, VOCs, NO<sub>x</sub>, and PM<sub>2.5</sub>. The uncounted wildfires emissions can lead to an underprediction in AODs. In addition, a constant, homogeneous PM<sub>2.5</sub> BCON of 8 µg m<sup>-3</sup> within 2-km of the surface and of values proportionally reduced above 2-km may not represent the large scale chemical transport events that affect the

model's capability in reproducing AODs, consistent with recent studies on the impacts of BCONs on chemical predictions [Tang *et al.*, 2007; Jimenez *et al.*, 2007]. Figure 19 shows the comparison between simulated total column AODs and observations from AERONET at four wavelengths (i.e., 0.3, 0.4, 0.6, 1.0 µm) and MODIS at a wavelength of 0.55 µm at Stennis, Mississippi (N 30 22' 04," W 89 37' 01"). The AERONET AODs at a wavelength of 0.6 µm are fairly consistent with MODIS AODs except on August 29. The model significantly underpredicts observed AODs at all wavelengths on August 28–29 and those at 0.3, 0.4, and 0.6 µm on August 31, for similar reasons stated previously.

## 4. Sensitivity Studies

### 4.1. Sensitivity of the Model Predictions to Gas/Particle Mass Transfer Approaches

[26] Although HYBR and KINE give an agreement between observed and simulated values that is similar to that for EQUI as shown in Figure 11 and the differences among

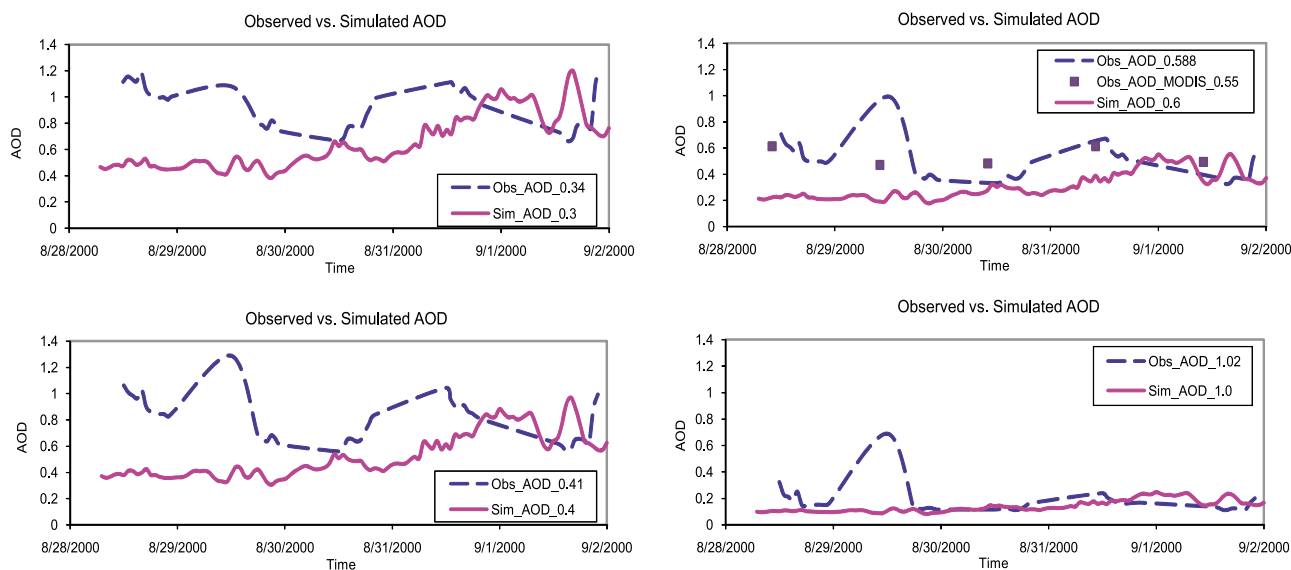
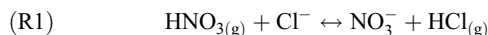


**Figure 19.** Simulated total column AOD versus observations from AERONET at four wavelengths (i.e., 0.3, 0.4, 0.6, 1.0  $\mu\text{m}$ ) and MODIS at one wavelength (i.e., 0.55  $\mu\text{m}$ ) at Stennis, Mississippi (N 30 22' 04," W 89 37' 01"). The simulated results are from WRF/Chem-MADRID (EQU).

the three sets of predictions with different gas/particle mass transfer approaches are small over the inland area, larger differences among them are found in the coastal area and over the sea. In particular, the simulation EQU gives much higher  $\text{PM}_{2.5}$  in the plume originating from Houston than those from HYBR and KINE. This trend can also be found in Figures 13 and 14, in which the three sets of predictions are close to each other at most sites except at GALC where EQU gives the highest  $\text{PM}_{2.5}$ .

[27] The high  $\text{PM}_{2.5}$  predictions by the equilibrium approach are attributed to high fine nitrate plume originating from the Houston area. The corresponding coarse nitrate concentrations are much lower than those predicted by the hybrid and kinetic approaches, as shown for August 30 in Figure 20. The coarse nitrate plume predicted by HYBR and KINE matches well with the coarse sodium ( $\text{Na}^+$ ) plume.  $\text{Na}^+$  is a tracer of sea-salt and it is emitted together with  $\text{Cl}^-$  from the ocean into the coarse mode using an online parameterization of Gong *et al.* [1997] that calculates sea-salt emissions as a function of WS10 in WRF/Chem. Several studies have reported that nitrate dominates in the coarse mode over coastal areas [Zhuang *et al.*, 1999; Bates *et al.*, 2008]. Nitrate can enter particulate phase through the chloride depletion process as follows [Zhuang *et al.*, 1999]:



The predicted coarse mode nitrate plume can thus be explained as the results of reactions between sea-salt and anthropogenic pollutant plume, which contains high concentrations of nitric acid ( $\text{HNO}_3$ ) (resulted from the oxidation of industry-emitted  $\text{NO}_x$ ). The high correlation between coarse mode nitrate and sodium predicted by HYBR and KINE indicates the occurrence of (R1). (R1) is included in the thermodynamic model ISORROPIA, which is used in MADRID. Since the hybrid and kinetic approaches both

solve the mass transfer for coarse particles kinetically, the  $\text{Cl}^-$  depletion process is correctly simulated. In the equilibrium approach, however, the particulate phase is treated together to equilibrate with the gas phase. Even though (R1) can still be simulated by the equilibrium approach, the transferred mass into particulate phase will be redistributed among each section based on initial sulfate distribution. Since most sulfate are in the accumulation mode, the transferred nitrate from the  $\text{Cl}^-$  depletion process will be artificially redistributed mostly to the accumulation mode, leading to high fine nitrate plume (rather than high coarse nitrate plume) originating from the Houston area by EQU. The reason explained above could be further confirmed by the simulated size-resolved PM composition distributions at a coastal site, GALC, where sea-salt emissions are high, although observed size-resolved composition is not available from TexAQS2000. As shown in Figure 21, chloride depletion process is captured correctly for the coarse sections with higher coarse nitrate that are solved kinetically in the hybrid and kinetic approaches. The equilibrium approach redistributes significant amounts of nitrate into fine mode, which artificially increases total  $\text{PM}_{2.5}$  concentrations (see Figure 11). Capaldo *et al.* [2000] and Athanasopoulou *et al.* [2008] also found such improper mass accumulation in the fine mode from predictions with the bulk equilibrium approach, while the kinetic approach is found to correctly predict nitrate predominantly in the coarse mode for the area affected by sea-salt emissions [Nolte *et al.*, 2008]. There are some sodium in section 6 (1.0–2.15  $\mu\text{m}$ ) at GALC, where the hybrid approach predicts less volatile species (i.e., nitrate and chloride) than the kinetic approach since the bulk equilibrium is used for the first 6 sections in the hybrid approach. Reducing the threshold cutoff diameter from 2.15 to 1  $\mu\text{m}$  may improve the performance of hybrid approach as shown by Hu *et al.* [2008]. On the other hand, as shown in Figure 14, since LaPorte is less impacted by sea-salt emissions and ammonium sulfate dominates the inorganic aerosol, no discernable

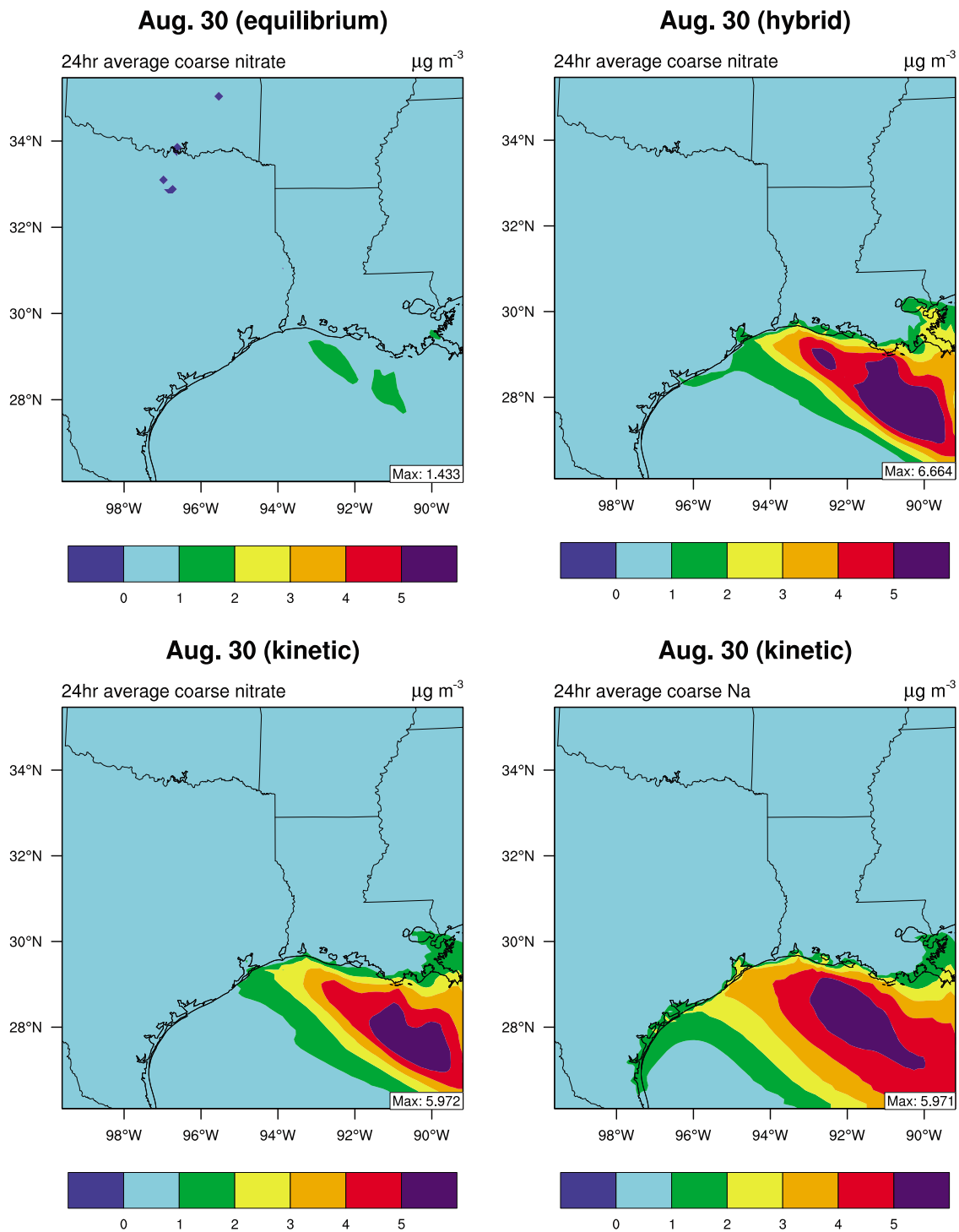


**Figure 20.** Daily average spatial distributions of simulated coarse nitrate concentrations on August 30, 2000 from WRF/Chem-MADRID (EQU), (HYBR), and (KINE) and sodium mass concentrations from WRF/Chem-MADRID (KINE).

differences can be found in the simulated nitrate and chloride concentrations by different mass transfer approaches.

#### 4.2. Aerosol Direct and Indirect Effects

[28] The presence of aerosols in the atmosphere will change the PBL meteorology and radiation budget through direct and indirect effects. As an online-coupled meteorology

and chemistry model, WRF/Chem can simulate such aerosol feedbacks and the net effects of aerosols can be obtained by conducting two simulations: with and without emissions of primary aerosols and formation of secondary aerosols. Figure 22 shows the difference in simulated net aerosol effects on September 1 which has the highest cloud coverage over domain during this episode. The net shortwave fluxes

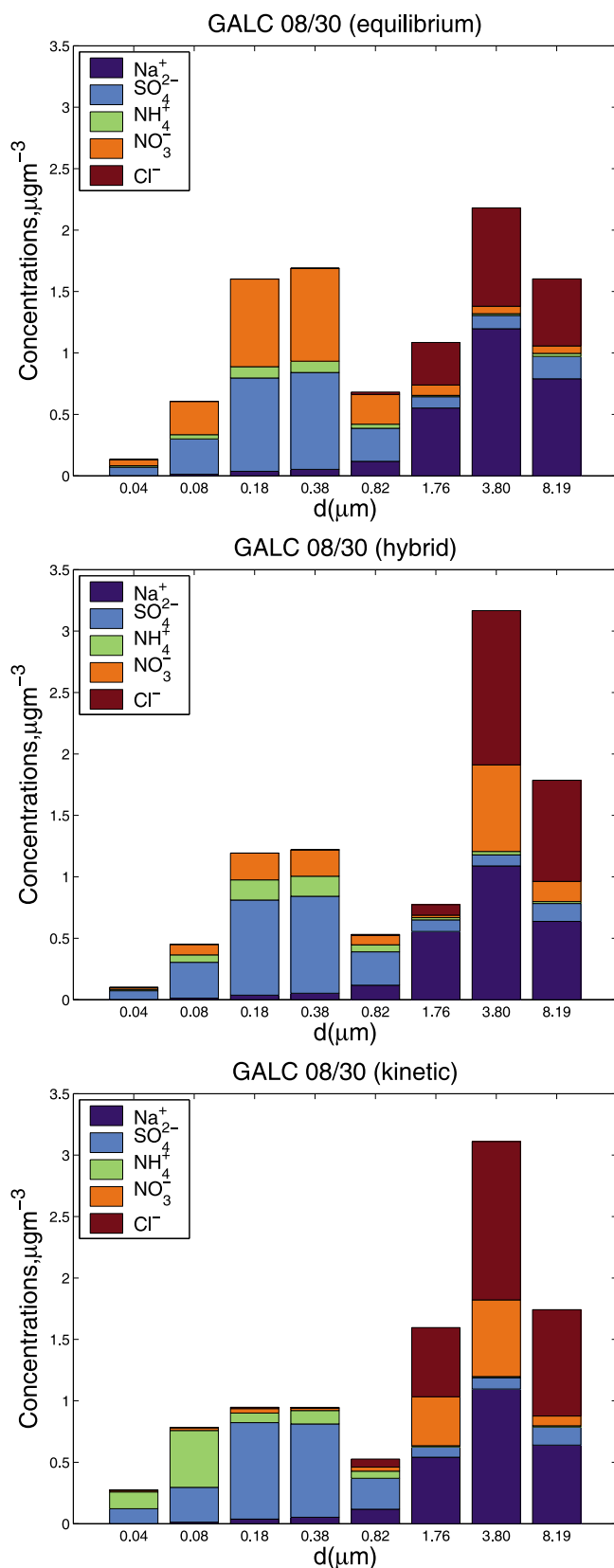


**Figure 21.** Predicted size-resolved PM compositions on August 30 at GALC from WRF/Chem-MADRID with different mass transfer approaches.

at surface are reduced by more than  $10 \text{ W m}^{-2}$  (or  $>3\%$ ) over the most of the areas with a domainwide mean reduction of  $14.4 \text{ W m}^{-2}$  (or  $>14.4\%$ ). Increases of  $>10 \text{ W m}^{-2}$  occur over some land (e.g., central Mississippi) or oceanic areas. This is mainly due to reduced cloud optical depths (as a result of reduced cloud coverage) during daytime. Near-surface temperatures are affected by several processes including net radiation at surface, convection and advection of air, and conductive heat transfer between surface and air. They either increase (up to  $1.4^\circ\text{C}$ ) or decrease (up to  $-1.3^\circ\text{C}$ ) in certain areas due to changes in these processes on September 1, with a net domainwide mean decrease of  $0.06^\circ\text{C}$ . While the decrease indicates a dominance of the effects due to reduced shortwave radiation, the increase indicates a dominance of the effect due to an increase in soil temperature as a result of decreased latent heat fluxes (thus an increase in the sensible heat flux from surface). Figure 23 shows the net effect of aerosols on vertical profile of temperatures at three sites in the Houston-Galveston area. At HOEA and H08H, temperatures decrease due to the cooling effect of aerosols at surface and below 600–800 mb but increase due to the warming effect of absorbing aerosols above 600–800 mb, such changes stabilize PBL and further exacerbate air pollution in this area. At GALC, temperatures at surface and below 600–800 mb also reduce but to a lesser extent on all days, indicating the effects of local sea-breezes and land-sea circulation on temperature profiles. In responses to increases or decreases in soil and air temperatures, soil moisture and water vapor in the air decrease or increase, respectively. Precipitation is affected by many cloud microphysical processes including the condensation of water vapor in clouds, collision and coalescence among the droplets, and turbulent mixing and entrainment in clouds and cloud-aerosol interactions such as activation of aerosols by cloud droplets. Large number concentration of small CCN in clouds (thus smaller mean drop size) may suppress precipitation, whereas giant CCN may enhance precipitation. As a net result, precipitation decreases or increases in some areas. Simulated surface CCN concentrations range from  $125$  to  $796 \text{ cm}^{-3}$  at a supersaturation of  $0.1\%$ , and from  $2060$  to  $53440 \text{ cm}^{-3}$  at a supersaturation of  $1\%$ , which is qualitatively consistent with the measured CCN concentrations over continents and oceans [Seinfeld and Pandis, 2006, and references therein]. The areas with high CCN coincide with areas with high  $\text{PM}_{2.5}$  concentrations as shown in Figure 11. The cloud droplet number concentrations (CDNC) can reach  $2064 \text{ cm}^{-3}$  on August 29–September 1 (see those on August 31 and September 1 in Figure 24). Simulated cloud coverage is much higher on August 31 and September 1 than on August 29–30, resulting in higher CDNC on both days, as shown in Figure 24.

## 5. Conclusions

[29] The aerosol module MADRID with improved gas/particle mass transfer approaches has been incorporated into WRF/Chem. The resulting model, WRF/Chem-MADRID, has been tested and evaluated with a 5-day episode from the TexAQS2000. WRF/Chem-MADRID simulates meteorological parameters reasonably well with MBs of  $0.5$ – $0.9^\circ\text{C}$  for T2,  $-18.3\%$  to  $5.7\%$  for RH2,  $0.3$  to  $-2.4 \text{ m s}^{-1}$  for WS10,  $20.5$  degree for WD10,  $0.06 \text{ mm day}^{-1}$  for Precip, and  $826.1 \text{ m}$  for the daytime PBLH. The larger positive

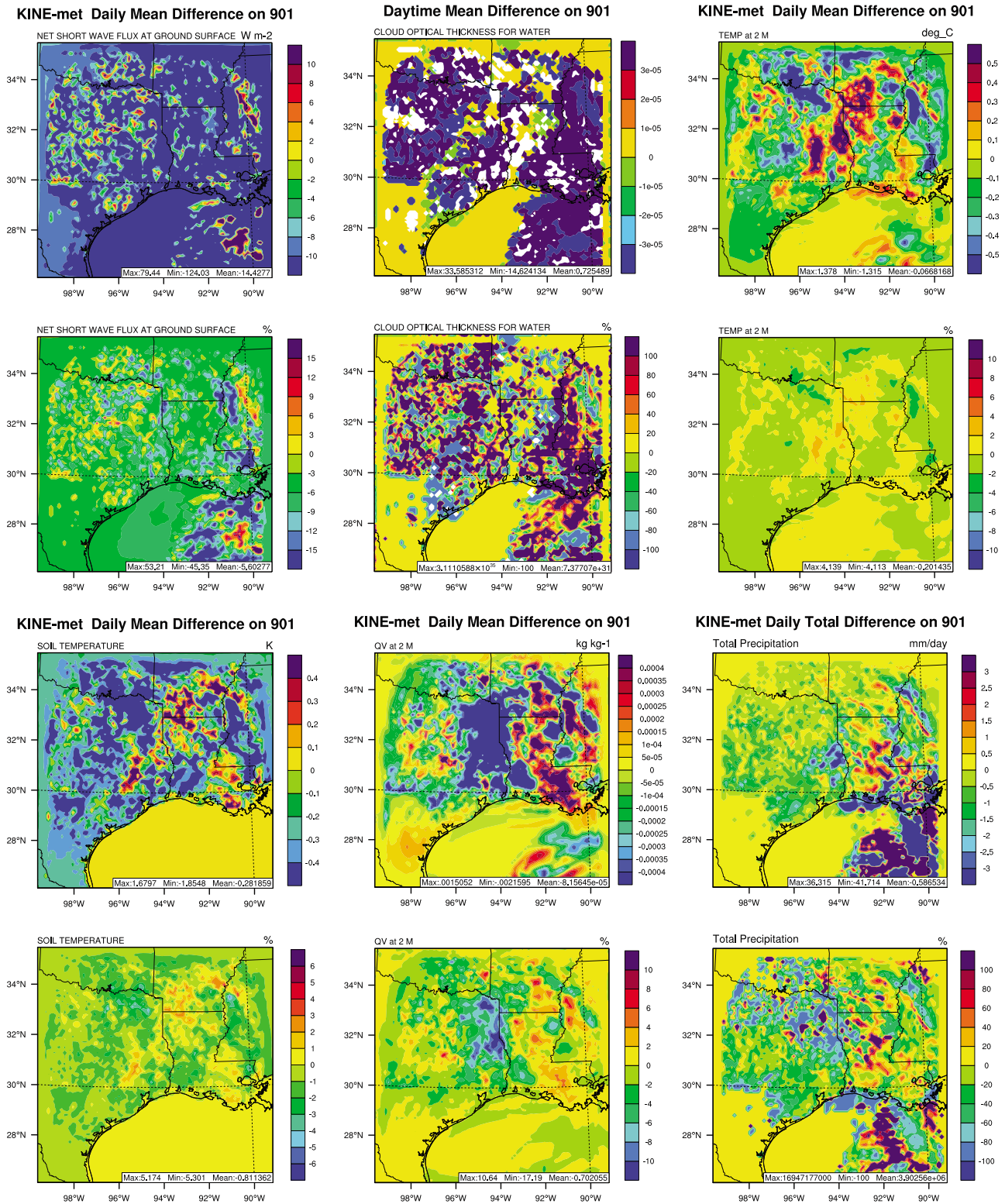


**Figure 22.** Absolute and percentage differences in daily mean net shortwave flux at surface, temperature at 2-m, latent heat flux at surface, water vapor mixing ratio, total precipitation and daytime mean (8 A.M.–7 P.M.) cloud optical depths due to the presence of aerosols. The simulation with aerosols is based on WRF/Chem-MADRID (KINE). The areas in white in the cloud optical depth plots indicate zero changes.

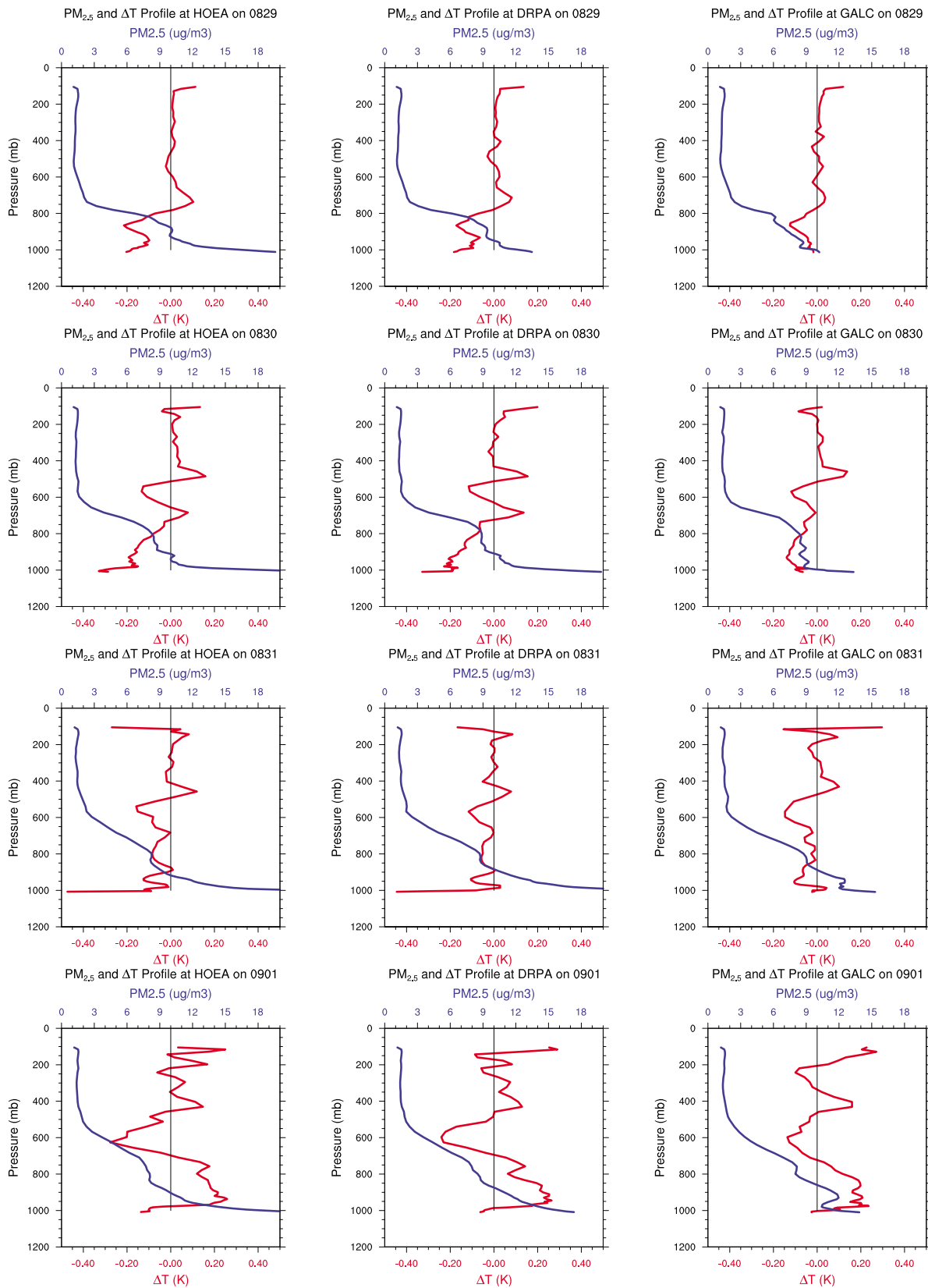


**Figure 23.** Vertical profiles of PM<sub>2.5</sub> simulated by WRF/Chem-MADRID (KINE) and vertical profiles of absolute difference of T and QV between simulations of WRF/Chem-MADRID and WRF only at four sites: HOEA, DPRA (or LaPorte), and GALC.

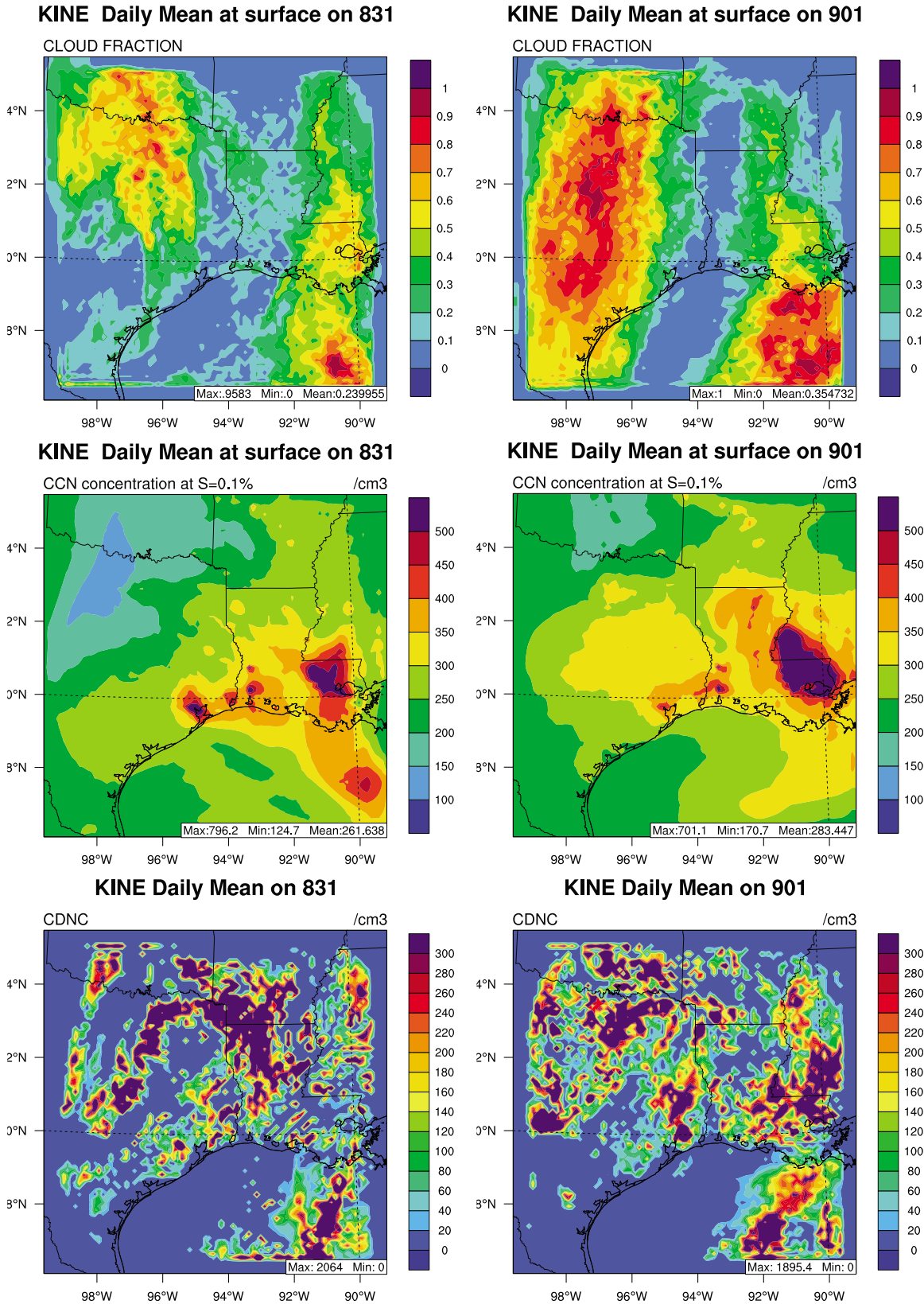


**Figure 24.** Simulated daily mean cloud fraction, cloud condensation nuclei, and cloud droplet number concentrations from WRF/Chem-MADRID (KINE) on August 31 and September 1, 2000.

biases in PBLH can be partially attributed to a possible underestimation due to the measurements obtained from wind profilers, in addition to uncertainties in model PBL treatments. The performance of some parameters (e.g., T2 and WS10) at night is worse than that during daytime. Sea/bay breeze development is overall captured by WRF/CHEM-MADRID but with a weaker penetration strength than observations. Simulated hourly  $O_3$  shows a high correlation coefficient (0.8) with observations and the overall mean bias is about 0.6 ppb. Some daily peak  $O_3$  mixing ratios are underpredicted, due possibly to uncertainties in the emissions of light olefins and their hourly variation, uncounted wildfire emissions, inaccurate predictions of small scale meteorological processes (e.g., mid-day PBLH and sea breezes), and missing of chlorine chemistry in the gas phase mechanism. WRF/CHEM-MADRID simulations with different gas/particle mass transfer approaches (EQUI, HYBR, and KINE) overpredict  $PM_{2.5}$  concentrations by 26.4%, 25.1%, and 28.1%, respectively. Simulated vertical profiles of temperature, RH, and concentrations of CO, NO,  $NO_2$ , and  $O_3$  are compared with aircraft measurements. The upper layer and column predictions such as TORs and AODs are also compared with satellite observations. While the model shows a reasonably good skill for predictions aloft, some large discrepancies exist between model results and observations, due to imperfectness in model treatments for upper layer meteorology, PBL processes and land-surface interactions, dynamics, and chemistry, uncounted wildfire emissions, and uncertainties in ICONs and BCONs aloft. The performance statistics for surface or near surface meteorological and chemical predictions are either similar or better than other modeling studies for the same episode using the same observational data set [e.g., *Fast et al.*, 2006], although the domains and horizontal resolutions for model evaluation were somewhat different among these studies. For example, the mean biases for T2, RH2, WS10, WD10, hourly  $O_3$  mixing ratio, and hourly  $PM_{2.5}$  concentrations simulated at the TCEQ sites are 0.9°C, -16.7%, -2.5 m s<sup>-1</sup>, 38.4°, 2 ppb, and 4  $\mu\text{g m}^{-3}$ , respectively, in the work by *Fast et al.* [2006], they are 0.5°C, -18.3%, 0.3 m s<sup>-1</sup>, and 20.5°, 0.6 ppb, and 2.7  $\mu\text{g m}^{-3}$ , respectively, in this work.

[30] The three gas/particle mass transfer approaches predict similar PM concentrations inland but EQUI predicts higher  $PM_{2.5}$  concentrations than HYBR and KINE over coastal areas, due to improperly redistributing condensed nitrate from the chloride depletion process to fine PM mode. Size-resolved aerosol measurements are not available from this episode to directly assess the performance in reproducing observed PM size distribution from the three gas/particle mass transfer approaches. WRF/CHEM-MADRID has also been applied to the 2004 New England Air Quality Study (NEAQS) episode, for which the size-resolved aerosol measurements are available for model evaluation. This NEAQS application shows better skills with hybrid and kinetic approaches in reproducing aerosol size/composition distribution over coastal areas, which will be presented in a separate paper. The CPU costs are 6.1, 8.4, and 10.2 h per simulation day for EQUI, HYBR, and KINE, respectively for this TeXAQS episode. The kinetic/APC and hybrid/APC approaches are therefore more accurate than EQUI yet sufficiently fast to provide accurate predictions of size-resolved  $PM_{2.5}$  over areas where anthropogenic emissions

mix with sea-salt emissions or sources for other reactive coarse PM (e.g., high emissions of dust).

[31] The presence of aerosols affects a number of radiative and meteorological variables. During the 5-day episode, the net shortwave fluxes at surface are reduced by more than 8 W m<sup>-2</sup> (or >3%) over most of the areas with a domain-mean reduction of 11.2–14.4 W m<sup>-2</sup> (or 4.1–5.6%) during this episode. Increases of >10 W m<sup>-2</sup> occur over some land or oceanic areas due mainly to reduced daytime cloud optical depths. Near-surface temperatures either increase or decrease with a net domainwide mean decrease of 0.06 to 0.14°C (0.2–0.42%) and up to 0.5°C at the individual sites in the Houston area during the episode, reflecting a dominance of the effects due to reduced shortwave radiation over the effect due to an increase in soil temperature. Simulated surface CCN concentrations range from 125 to 796 cm<sup>-3</sup> at a supersaturation of 0.1% and 2060 to 53440 cm<sup>-3</sup> at a supersaturation of 1%. Simulated CDNC can reach 2064 cm<sup>-3</sup> on August 29–September 1. As a net effect of changes in cloud properties, precipitation decreases or increases with a domainwide mean reduction of 0.22–0.59 mm day<sup>-1</sup>. While these results show importance of aerosol direct and indirect effects, uncertainties may exist in their magnitudes and signs as the biases in simulated  $PM_{2.5}$  mass concentrations and size-resolved compositions may propagate into simulated aerosol effects. Although the simulated feedback effects on a short time scale may differ from feedbacks on a longer time scale, they indicate the importance of quantifying aerosol direct and indirect effects to better understand their roles in climate change.

[32] **Acknowledgments.** This work was performed at NCSU under the National Science Foundation Career Award Atm-0348819, the Memorandum of Understanding between the U.S. Environmental Protection Agency (EPA) and the U.S. Department of Commerce's National Oceanic and Atmospheric Administration (NOAA) and under agreement DW13921548, and the U.S. EPA-Science to Achieve Results (STAR) program (grant RD833376). Thanks are due to Naresh Kumar and Eladio Knipping, EPRI and Christian Seigneur, formerly at AER and now at CEREA, France, for permitting the use of original version of MADRID code for NCSU's further improvement and incorporation into WRF/Chem; Mark Z. Jacobson, Stanford University, for providing APC and coagulation source codes for the improvement of MADRID; and Richard C. Easter and Rahul Zaveri, PNNL, for helpful discussions on MADRID incorporation and the conversion code from FORTRAN 77/90 fixed format to FORTRAN 90 free format. Thanks are also due to Xiao-Ming Hu, a former student at NCSU, for his work on the incorporation of an earlier version of MADRID into WRF/Chem v2.2 and scripts for post-processing model results. Thanks are also due to Mark Estes, TCEQ, for providing observational data from TexAQS2000 collected by TCEQ; Jack Fishman and John K. Creilson, NASA Langley Research Center, for providing TOR data; D. Allen Chu, NASA Goddard Space Flight Center, for providing AERONET data at Stennis, Mississippi and MODIS-derived AOD data; Shao-Cai Yu, the U.S. EPA, for providing the script for statistical calculation and aircraft data extraction; Alice Gilliland and Steve Howard, U.S. EPA, for providing observations from AIRS-AQS and CASTNET; Steven Peckham and Stuart McKeen, NOAA/ESRL, for helpful discussions on WRF/Chem.

## References

- Allen, D. T., and M. P. Fraser (2006), An overview of the Gulf Coast Aerosol Research and Characterization Study: The Houston PM Super-site, *J. Air Waste Manage. Assoc.*, 56, 456–466.
- Al-Saadi, J., et al. (2005), Improving national air quality forecasts with satellite aerosol observations, *Bull. Am. Meteorol. Soc.*, 86(9), 1249–1261, doi:10.1175/BAMS-86-9-1249.

- Angevine, W. M., M. Tjernstrom, and M. Zagar (2006), Modeling of the coastal boundary layer and pollutant transport in New England, *J. Appl. Meteorol. Climatol.*, *45*, 137–154, doi:10.1175/JAM2333.1.
- Athanasopoulou, E., M. Tombrou, S. N. Pandis, and A. G. Russell (2008), The role of sea-salt emissions and heterogeneous chemistry in the air quality of polluted coastal areas, *Atmos. Chem. Phys. Discuss.*, *8*, 3807–3841, doi:10.5194/acpd-8-3807-2008.
- Banta, R. M., C. J. Seniff, J. Nielsen-Gammon, L. S. Darby, T. B. Ryerson, R. J. Alvarez, S. P. Sandberg, E. J. Williams, and M. Trainer (2005), A bad air day in Houston, *Bull. Am. Meteorol. Soc.*, *86*, 657–669, doi:10.1175/BAMS-86-5-657.
- Bao, J.-W., S. A. Michelson, S. A. McKeen, and G. A. Grell (2005), Meteorological evaluation of a weather-chemistry forecasting model using observations from the TEXAS AQS 2000 field experiment, *J. Geophys. Res.*, *110*, D21105, doi:10.1029/2004JD005024.
- Bates, T. S., et al. (2008), Boundary layer aerosol chemistry during TexAQS/GoMACCS 2006: Insights into aerosol sources and transformation processes, *J. Geophys. Res.*, *113*, D00F01, doi:10.1029/2008JD010023 [printed 115(D7), 2010].
- Capaldo, K. P., C. Pilinis, and S. N. Pandis (2000), A computationally efficient hybrid approach for dynamic gas/aerosol transfer in air quality models, *Atmos. Environ.*, *34*, 3617–3627, doi:10.1016/S1352-2310(00)00092-3.
- Chang, S., and D. T. Allen (2006), Atmospheric chlorine chemistry in southeast Texas: Impacts on ozone formation and control, *Environ. Sci. Technol.*, *40*, 251–262, doi:10.1021/es050787z.
- Chang, S., E. McDonald-Buller, Y. Kimura, G. Yarwood, J. Neece, M. Russell, P. Tanaka, and D. Allen (2002), Sensitivity of urban ozone formation to chlorine emission estimates, *Atmos. Environ.*, *36*, 4991–5003, doi:10.1016/S1352-2310(02)00573-3.
- Chapman, E. G., W. I. Gustafson Jr., R. C. Easter, J. C. Barnard, S. J. Ghan, M. S. Pekour, and J. D. Fast (2008), Coupling aerosol-cloud-radiative processes in the WRF-Chem model: Investigating the radiative impact of elevated point sources, *Atmos. Chem. Phys. Discuss.*, *8*, 14,765–14,817, doi:10.5194/acpd-8-14765-2008.
- Chu, D. A., Y. J. Kaufman, G. Zibordi, J. D. Chern, J. Mao, C. Li, and B. N. Holben (2003), Global monitoring of air pollution over land from the Earth Observing System-Terra Moderate Resolution Imaging Spectroradiometer (MODIS), *J. Geophys. Res.*, *108*(D21), 4661, doi:10.1029/2002JD003179.
- Colby, F. P., Jr. (2004), Simulation of the New England sea breeze: The effect of grid spacing, *Weather Forecast.*, *19*, 277–285, doi:10.1175/1520-0434(2004)019<0277:SOTNES>2.0.CO;2.
- Darby, L. S. (2005), Cluster analysis of surface winds in Houston, Texas, and the impact of wind patterns on ozone, *J. Appl. Meteorol.*, *44*, 1788–1806, doi:10.1175/JAM2320.1.
- Daum, P. H., L. I. Kleinman, S. R. Springston, L. J. Nunnermacker, Y.-N. Lee, J. Weinstein-Lloyd, J. Zheng, and C. M. Berkowitz (2003), A comparative study of O<sub>3</sub> formation in the Houston urban and industrial plumes during the 2000 Texas Air Quality Study, *J. Geophys. Res.*, *108*(D23), 4715, doi:10.1029/2003JD003552.
- Daum, P. H., L. I. Kleinman, S. R. Springston, L. J. Nunnermacker, Y.-N. Lee, J. Weinstein-Lloyd, J. Zheng, and C. M. Berkowitz (2004), Origin and properties of plumes of high ozone observed during the Texas 2000 Air Quality Study (TexAQS 2000), *J. Geophys. Res.*, *109*, D17306, doi:10.1029/2003JD004311.
- Fast, J. D., W. I. Gustafson Jr., R. C. Easter, R. A. Zaveri, J. C. Barnard, E. G. Chapman, G. A. Grell, and S. E. Peckham (2006), Evolution of ozone, particulates, and aerosol direct radiative forcing in the vicinity of Houston using a fully coupled meteorology-chemistry-aerosol model, *J. Geophys. Res.*, *111*, D21305, doi:10.1029/2005JD006721.
- Frost, G. J., et al. (2006), Effects of changing power plant NO<sub>x</sub> emissions on ozone in the eastern United States: Proof of concept, *J. Geophys. Res.*, *111*, D12306, doi:10.1029/2005JD006354.
- Gaydos, T. M., B. Koo, S. N. Pandis, and D. P. Chock (2003), Development and application of an efficient moving sectional approach for the solution of the atmospheric aerosol condensation/evaporation equations, *Atmos. Environ.*, *37*, 3303–3316.
- Gong, S. L., L. A. Barrie, and J.-P. Blanchet (1997), Modeling sea-salt aerosols in the atmosphere: 1. Model development, *J. Geophys. Res.*, *102*, 3805–3818, doi:10.1029/96JD02953.
- Grell, G. A., S. E. Peckham, R. Schmitz, S. A. McKeen, G. Frost, W. C. Skamarock, and B. Eder (2005), Fully coupled “on-line” chemistry within the WRF model, *Atmos. Environ.*, *39*, 6957–6975, doi:10.1016/j.atmosenv.2005.04.027.
- Grossman-Clarke, S., J. A. Zehnder, W. L. Stefanov, Y. Liu, and M. A. Zoldak (2005), Urban modifications in a mesoscale meteorological model and the effects on near-surface variables in an arid metropolitan region, *J. Appl. Meteorol.*, *44*(9), 1281–1297, doi:10.1175/JAM2286.1.
- Heald, C. L., D. J. Jacob, R. J. Park, B. Alexander, T. D. Fairlie, R. M. Yantosca, and D. A. Chu (2006), Transpacific transport of Asian anthropogenic aerosols and its impact on surface air quality in the United States, *J. Geophys. Res.*, *111*, D14310, doi:10.1029/2005JD006847.
- Hong, S. Y., Y. Noh, and J. Dudhia (2006), A new vertical diffusion package with explicit treatment of entrainment processes, *Mon. Weather Rev.*, *134*(9), 2318–2341, doi:10.1175/MWR3199.1.
- Hu, X.-M. (2008), Incorporation of the Model of Aerosol Dynamics, Reaction, Ionization, and Dissolution (MADRID) into the Weather Research and Forecasting Model with Chemistry (WRF/Chem): Model development and retrospective applications, Ph.D. dissertation, N. C. State Univ., Raleigh, July.
- Hu, X.-M., Y. Zhang, M. Z. Jacobson, and C. K. Chan (2008), Coupling and evaluating gas/particle mass transfer treatments for aerosol simulation and forecast, *J. Geophys. Res.*, *113*, D11208, doi:10.1029/2007JD009588.
- Hutchison, K. D., S. Faruqui, and S. Smith (2008), Improving correlations between MODIS aerosol optical thickness and ground-based PM<sub>2.5</sub> observations through 3D spatial analyses, *Atmos. Environ.*, *42*(3), 530–543, doi:10.1016/j.atmosenv.2007.09.050.
- Jacobson, M. Z. (2005), A solution to the problem of nonequilibrium acid/base gas-particle transfer at long time step, *Aerosol Sci. Technol.*, *39*, 92–103, doi:10.1080/027868290904546.
- Jacobson, M. Z., R. P. Turco, E. J. Jensen, and O. B. Toon (1994), Modeling coagulation among particles of different composition and size, *Atmos. Environ.*, *28*, 1327–1338, doi:10.1016/1352-2310(94)90280-1.
- Jiang, G. F., and J. D. Fast (2004), Modeling the effects of VOC and NO<sub>x</sub> emission sources on ozone formation in Houston during the Tex-AQS 2000 field campaign, *Atmos. Environ.*, *38*, 5071–5085, doi:10.1016/j.atmosenv.2004.06.012.
- Jimenez, P., R. Parra, and J. M. Baldasano (2007), Influence of initial and boundary conditions for ozone modeling in very complex terrains: A case study in the northeastern Iberian Peninsula, *Environ. Model. Softw.*, *22*(9), 1294–1306, doi:10.1016/j.envsoft.2006.08.004.
- Junquera, V., M. M. Russell, W. Vizuete, Y. Kimura, and D. Allen (2005), Wildfires in eastern Texas in August and September 2000: Emissions, aircraft measurements, and impact on photochemistry, *Atmos. Environ.*, *39*, 4983–4996, doi:10.1016/j.atmosenv.2005.05.004.
- Karl, T., et al. (2003), Use of proton-transfer-reaction mass spectrometry to characterize volatile organic compound sources at the La Porte super site during the Texas Air Quality Study 2000, *J. Geophys. Res.*, *108*(D16), 4508, doi:10.1029/2002JD003333.
- Kleinman, L. I., P. H. Daum, D. G. Imre, Y.-N. Lee, L. J. Nunnermacker, S. R. Springston, J. Weinstein-Lloyd, and J. Rudolph (2002), Ozone production rate and hydrocarbon reactivity in 5 urban areas: A cause of high ozone concentration in Houston, *Geophys. Res. Lett.*, *29*(10), 1467, doi:10.1029/2001GL014569.
- Kleinman, L. I., P. H. Daum, Y.-N. Lee, L. J. Nunnermacker, S. R. Springston, J. Weinstein-Lloyd, and J. Rudolph (2005), A comparative study of ozone production in five U.S. metropolitan areas, *J. Geophys. Res.*, *110*, D02301, doi:10.1029/2004JD005096.
- Koo, B., T. M. Gaydos, and S. N. Pandis (2003), Evaluation of the equilibrium, dynamic, and hybrid aerosol modeling approaches, *Aerosol Sci. Technol.*, *37*, 53–64, doi:10.1080/02786820300893.
- Lee, J. H., P. K. Hopke, T. M. Holsen, and A. V. Polissar (2005), Evaluation of continuous and filter-based methods for measuring PM<sub>2.5</sub> mass concentration, *Aerosol Sci. Technol.*, *39*, 290–303, doi:10.1080/027868290929323.
- Lemire, K. R., D. T. Allen, G. A. Klouda, and C. W. Lewis (2002), Fine particulate matter source attribution for southeast Texas using <sup>14</sup>C/<sup>13</sup>C ratios, *J. Geophys. Res.*, *107*(D22), 4613, doi:10.1029/2002JD002339.
- Levy, R. C., L. A. Remer, S. Mattoo, E. F. Vermote, and Y. J. Kaufman (2007), Second-generation operational algorithm: Retrieval of aerosol properties over land from inversion of Moderate Resolution Imaging Spectroradiometer spectral reflectance, *J. Geophys. Res.*, *112*, D13211, doi:10.1029/2006JD007811.
- McKeen, S., et al. (2005), Assessment of an ensemble of seven real-time ozone forecasts over eastern North America during the summer of 2004, *J. Geophys. Res.*, *110*, D21307, doi:10.1029/2005JD005858.
- McKeen, S., et al. (2007), Evaluation of several PM<sub>2.5</sub> forecast models using data collected during the ICARTT/NEAQS 2004 field study, *J. Geophys. Res.*, *112*, D10S20, doi:10.1029/2006JD007608.
- McMurry, P. H., and S. K. Friedlander (1979), New particle formation in the presence of an aerosol, *Atmos. Environ.*, *13*, 1635–1651, doi:10.1016/0004-6981(79)90322-6.
- Misenis, C., and Y. Zhang (2010), An examination of WRF/Chem: Physical parameterizations, nesting options, and grid resolutions, *Atmos. Res.*, *97*, 315–334, doi:10.1016/j.atmosres.2010.04.005.
- Murphy, C. F., and D. T. Allen (2005), Hydrocarbon emissions from industrial release events in the Houston-Galveston area and their impact

- on ozone formation, *Atmos. Environ.*, 39(21), 3785–3798, doi:10.1016/j.atmosenv.2005.02.051.
- Nam, J., Y. Kimura, W. Vizuete, C. F. Murphy, and D. T. Allen (2006), Modeling the impacts of emission events on ozone formation in Houston, Texas, *Atmos. Environ.*, 40(28), 5329–5341, doi:10.1016/j.atmosenv.2006.05.002.
- Nenes, A., C. Pilinis, and S. N. Pandis (1998), ISORROPIA: A new thermodynamic equilibrium model for multiphase multicomponent marine aerosols, *Aquat. Geochem.*, 4, 123–152, doi:10.1023/A:1009604003981.
- Nolte, C. G., P. V. Bhave, J. R. Arnold, R. L. Dennis, K. M. Zhang, and A. S. Wexler (2008), Modeling urban and regional aerosols—Application of the CMAQ-UCD aerosol model to Tampa, a coastal urban site, *Atmos. Environ.*, 42, 3179–3191, doi:10.1016/j.atmosenv.2007.12.059.
- Pavlovic, R. T., U. Nopmongcol, Y. Kimura, and D. T. Allen (2006), Ammonia emissions, concentrations and implications for particulate matter formation in Houston, Texas, *Atmos. Environ.*, 40, suppl. 2, 538–551, doi:10.1016/j.atmosenv.2006.04.071.
- Pun, B. K., C. Seigneur, J. Pankow, E. Chang, R. Griffin, and E. Knipping (2005), An upgraded absorptive secondary organic aerosol partitioning module for three-dimensional air quality applications, paper 7B4 presented at the 24th Annual AAAR Conference, Am. Assoc. for Aerosol Res., Austin, Tex., Oct.
- Russell, M., and D. T. Allen (2004), Seasonal and spatial trends in primary and secondary organic carbon concentrations in southeast Texas, *Atmos. Environ.*, 38, 3225–3239, doi:10.1016/j.atmosenv.2004.03.013.
- Russell, M. M., D. T. Allen, D. R. Collins, and M. P. Fraser (2004), Daily, seasonal, and spatial trends in PM<sub>2.5</sub> mass and composition in southeast Texas, *Aerosol Sci. Technol.*, 38(S1), 14–26, doi:10.1080/02786820390229318.
- Ryerson, T. B., et al. (2003), Effect of petrochemical industrial emissions of reactive alkenes and NO<sub>x</sub> on tropospheric ozone formation in Houston, Texas, *J. Geophys. Res.*, 108(D8), 4249, doi:10.1029/2002JD003070.
- Sarwar, G., D. Luecken, G. Yarwood, G. Z. Whitten, and W. P. L. Carter (2008), Impact of an updated carbon bond mechanism on predictions from the CMAQ modeling system: Preliminary assessment, *J. Appl. Meteorol. Climatol.*, 47, 3–14, doi:10.1175/2007JAMC1393.1.
- Schell, B., I. J. Ackermann, H. Hass, F. S. Binkowski, and A. Ebel (2001), Modeling the formation of secondary organic aerosol within a comprehensive air quality model system, *J. Geophys. Res.*, 106, 28,275–28,293.
- Seibert, P., F. Beyrich, S.-E. Gryning, S. Joffre, A. Rasmussen, and P. Tercier (2000), Review and intercomparison of operational methods for the determination of the mixing height, *Atmos. Environ.*, 34, 1001–1027, doi:10.1016/S1352-2310(99)00349-0.
- Seigneur, C., et al. (2000), Guidance for the performance evaluation of three-dimensional air quality modeling systems for particulate matter and visibility, *J. Air Waste Manage. Assoc.*, 50, 588–599.
- Seinfeld, J. H., and S. Pandis (2006), *Atmospheric Chemistry and Physics: From Air Pollution to Climate Change*, 2nd ed., 1203 pp., John Wiley, New York.
- Stockwell, W. R., P. Middleton, J. S. Chang, and X. Tang (1990), The second generation regional acid deposition model chemical mechanism for regional air quality modeling, *J. Geophys. Res.*, 95, 16,343–16,367, doi:10.1029/JD095iD10p16343.
- Tanaka, P. L., et al. (2003), Direct evidence for chlorine-enhanced urban ozone formation in Houston, Texas, *Atmos. Environ.*, 37, 1393–1400, doi:10.1016/S1352-2310(02)01007-5.
- Tang, Y., et al. (2007), Influence of lateral and top boundary conditions on regional air quality prediction: A multiscale study coupling regional and global chemical transport models, *J. Geophys. Res.*, 112, D10S18, doi:10.1029/2006JD007515.
- Tombette, M., and B. Sportisse (2007), Aerosol modeling at a regional scale: Model-to-data comparison and sensitivity analysis over greater Paris, *Atmos. Environ.*, 41, 6941–6950, doi:10.1016/j.atmosenv.2006.10.037.
- Vizuete, W. (2005), Implementation of process analysis in a three dimensional air quality model, Ph.D. thesis, 240 pp., Univ. of Tex., Austin.
- Webster, M., J. Nam, Y. Kimura, H. Jeffries, W. Vizuete, and D. T. Allen (2007), The effect of variability in industrial emissions on ozone formation in Houston, Texas, *Atmos. Environ.*, 41(40), 9580–9593, doi:10.1016/j.atmosenv.2007.08.052.
- Wert, B. P., et al. (2003), Signatures of terminal alkene oxidation in airborne formaldehyde measurements during TexAQS 2000, *J. Geophys. Res.*, 108(D3), 4104, doi:10.1029/2002JD002502.
- Zaveri, R. A., and L. K. Peters (1999), A new lumped structure photochemical mechanism for large-scale applications, *J. Geophys. Res.*, 104, 30,387–30,415, doi:10.1029/1999JD900876.
- Zaveri, R. A., R. C. Easter, J. D. Fast, and L. K. Peters (2008), Model for Simulating Aerosol Interactions and Chemistry (MOSAIC), *J. Geophys. Res.*, 113, D13204, doi:10.1029/2007JD008782.
- Zhang, Y., C. Seigneur, J. H. Seinfeld, M. Jacobson, and F. S. Binkowski (1999), Simulation of aerosol dynamics: A comparative review of algorithms used in air quality models, *Aerosol Sci. Technol.*, 31(6), 487–514, doi:10.1080/027868299304039.
- Zhang, Y., B. Pun, K. Vijayaraghavan, S.-Y. Wu, C. Seigneur, S. Pandis, M. Jacobson, A. Nenes, and J. H. Seinfeld (2004), Development and application of the model of aerosol dynamics, reaction, ionization and dissolution (MADRID), *J. Geophys. Res.*, 109, D01202, doi:10.1029/2003JD003501.
- Zhang, Y., P. Liu, B. Pun, and C. Seigneur (2006), A comprehensive performance evaluation of MM5-CMAQ for the summer 1999 Southern Oxidants Study episode—Part I: Evaluation protocols, databases and meteorological predictions, *Atmos. Environ.*, 40, 4825–4838, doi:10.1016/j.atmosenv.2005.12.043.
- Zhang, Y., X.-Y. Wen, K. Wang, K. Vijayaraghavan, and M. Z. Jacobson (2009), Probing into regional O<sub>3</sub> and particulate matter pollution in the United States: 2. An examination of formation mechanisms through a process analysis technique and sensitivity study, *J. Geophys. Res.*, 114, D22305, doi:10.1029/2009JD011900.
- Zhang, Y., P. Liu, X.-H. Liu, B. Pun, C. Seigneur, M. Z. Jacobson, and W.-X. Wang (2010a), Fine-scale modeling of wintertime aerosol mass, number, and size distributions in central California, *J. Geophys. Res.*, 115, D15207, doi:10.1029/2009JD012950.
- Zhang, Y., X.-Y. Wen, and C. J. Jang (2010b), Simulating climate-chemistry-aerosol-cloud-radiation feedbacks in continental U.S. using online-coupled WRF/Chem, *Atmos. Environ.*, 44(29), 3568–3582.
- Zhuang, H., C. K. Chan, M. Fang, and A. S. Wexler (1999), Formation of nitrate and non-sea-salt sulfate on coarse particles, *Atmos. Environ.*, 33, 4223–4233, doi:10.1016/S1352-2310(99)00186-7.

J. D. Fast, Pacific Northwest National Laboratory, Richland, WA 99352, USA.

G. A. Grell, Earth Systems Research Laboratory, NOAA, Boulder, CO 80305, USA.

Y. Pan, K. Wang, and Y. Zhang, Department of Marine, Earth and Atmospheric Sciences, North Carolina State University, Campus Box 8208, Raleigh, NC 27606, USA. (yang\_zhang@ncsu.edu)